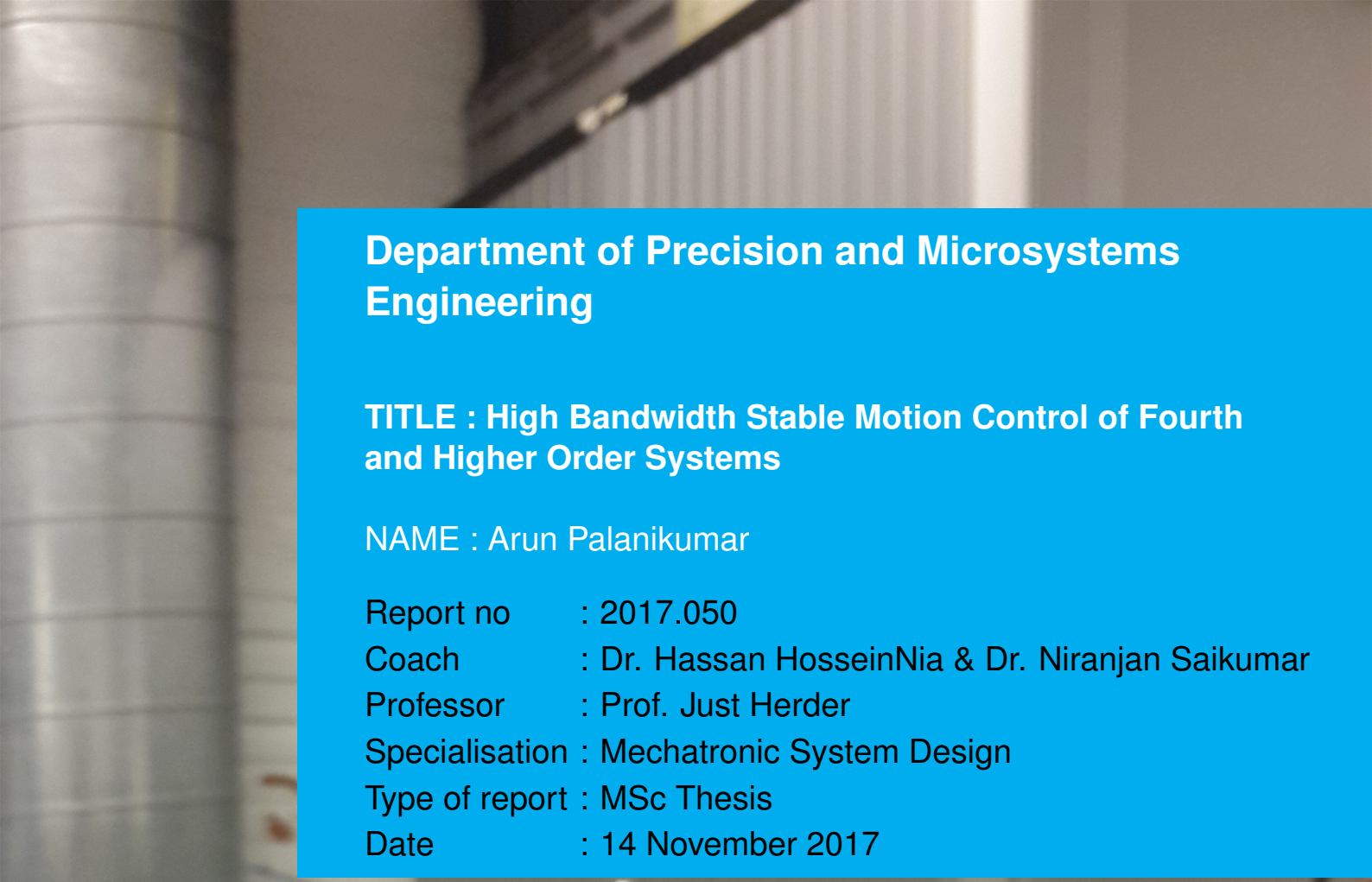

Department of Precision and Microsystems Engineering

TITLE : High Bandwidth Stable Motion Control of Fourth and Higher Order Systems

NAME : Arun Palanikumar

Report no : 2017.050
Coach : Dr. Hassan HosseinNia & Dr. Niranjan Saikumar
Professor : Prof. Just Herder
Specialisation : Mechatronic System Design
Type of report : MSc Thesis
Date : 14 November 2017

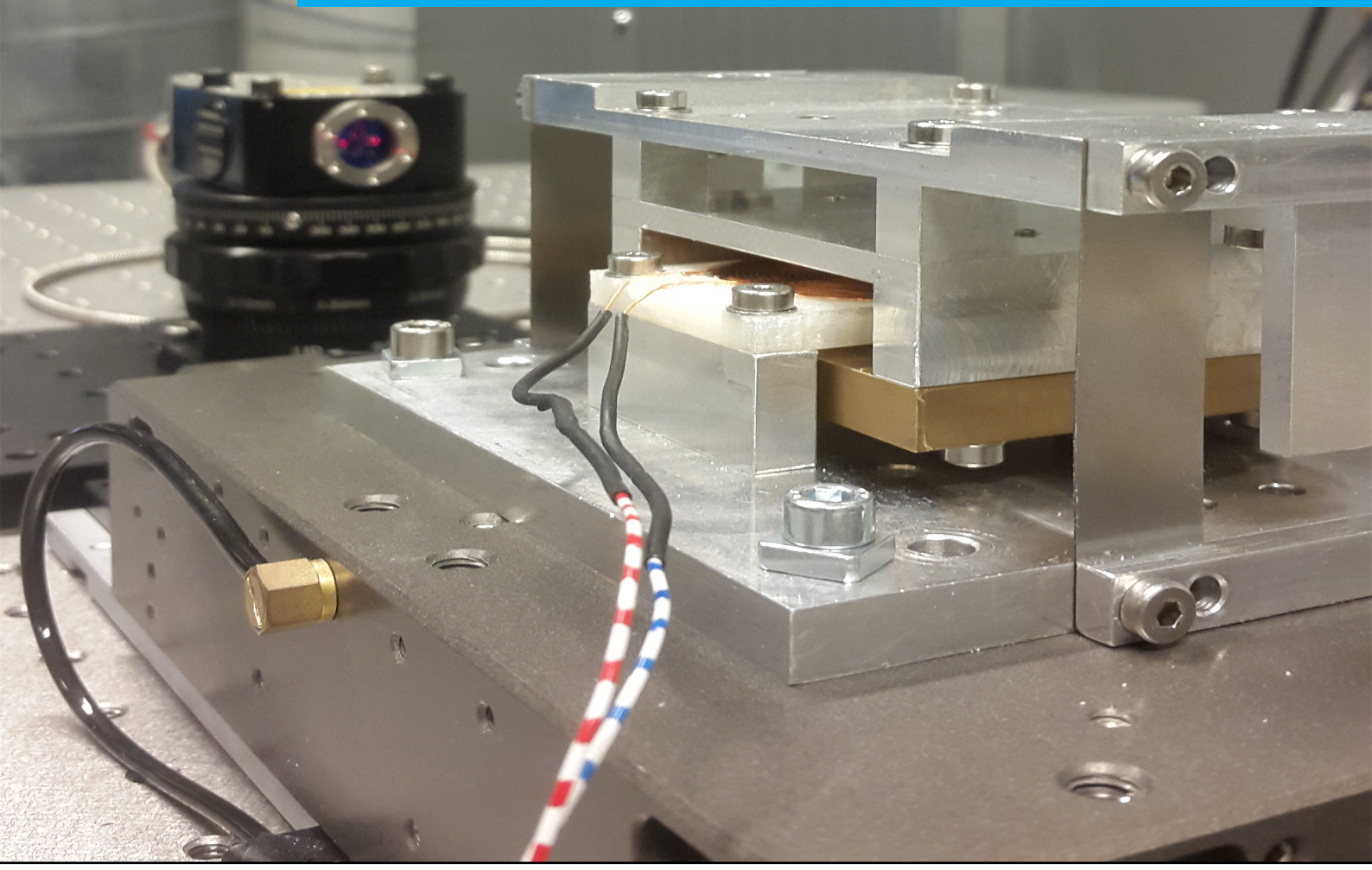

High Bandwidth Stable Motion Control of Fourth and Higher Order Systems

by

Arun Palanikumar

in partial fulfillment of the requirements for the degree of

Master of Science

in Mechanical Engineering

at the Delft University of Technology,

to be defended publicly on Friday November 24,2017 at 10:00 AM.

Supervisor:	Dr. Hassan HosseinNia
	Dr. Niranjan Saikumar
Thesis committee:	Prof.dr.ir. J.L. Herder (chairman)
	Dr. S.H. Hossein Nia Kani
	Dr.ir. J.F.L. Goosen
	Dr. Niranjan Saikumar

TU Delft Delft University of Technology

PREFACE

This work is a part of master programme of Arun Palanikumar and is dedicated to wards the fulfillment of the degree of Master of Science in Mechanical Engineering at the Precision and Microsystems Engineering group of Delft University of Technology (TU Delft), with specialization in mechatronic system design. This research has been conducted at the facilities of TU Delft, under the expert guidance and supervision of mentors at TU Delft.

Arun Palanikumar
Delft,November 13, 2017

ACKNOWLEDGEMENT

The last two years of my life spent in the Netherlands, and at TU Delft has been a valuable experience in my life. I would like to thank the following people for their contributions during my thesis work.

Niranjan Saikumar, for being there whenever I needed help with anything. Your thorough knowledge and comprehension of the subject helped me gain clarity in the thesis on numerous occasions.

Hassan HosseinNia, first of all, for being my supervisor. I really appreciate the way you guided this thesis work, giving me enough freedom, correcting me when I was wrong, and always keeping the research in focus.

Jo Spronck, for your valuable contributions at various stages of the thesis. You challenged the way I think, and encouraged bringing in out-of-the-box solutions.

Rob Luttjeboer and Patrick van Holst for your invaluable support in the lab, helping me on time with everything I needed.

Linda Chen for all the long hours spent in the lab trying to get our setup working, and for being understanding in fixing schedules.

Bart Joziasse for patiently getting me familiarized with the setup and with dSPACE, and for answering questions throughout the year.

All my fellow MSD students and PhD candidates for your inputs and advice during the Monday meetings, providing outside perspectives and inputs which helped me think about my work from various angles.

ABSTRACT

The high tech industry is at the forefront of pushing the limitations and barriers in motion control technology. Demands for achieving higher precision and speeds are ever increasing. The wafer scanner industry, which is involved in manufacturing integrated circuits, is a prime example where (sub) nanometer precision positioning is required, while at the same time meeting challenging throughput demands. PID control technique has been the standard for industrial motion control for many years. With multiple advancements in the feedforward control techniques, it has become possible to achieve very high bandwidths and precision. However, PID control, being a linear control technique, has inherent design limitations such as the 'water-bed effect', due to which the requirements in terms of robustness and precision become conflicting in nature, thus making a trade-off inevitable. Due to this, improving one performance criterion without negatively influencing the other is impossible. Such limitations become more evident when the severity of the demands increases. Thus there is a need to find ways to overcome such limitations.

This MSc thesis focuses on PID control, keeping in mind the prevalence of the technique in motion control and its wide applicability. In order to overcome the limitations of linear control, it is clear that it is necessary to look into nonlinear control methods. Reset control, one such nonlinear technique, is identified to be readily compatible with the PID control scheme. In reset control, the controller states are reset when the error between the reference signal and the output becomes zero. Studying the frequency domain properties of reset control using describing function analysis, it is observed that reset elements have lesser phase lag for similar gain behavior when compared to their linear counterparts. For example, a reset integrator shows a phase lag of about 38 degrees, which is 52 degrees lesser than a linear integrator. This is not possible with linear control, as explained by Bode's gain phase relationship. Thus, this thesis focuses on implementing reset in PID control scheme, so as to lessen the severity of waterbed effect and to improve bandwidth and precision of motion control systems.

Describing function analysis is used to approximate the phase advantage achieved, and to obtain a better open loop shape in comparison to a PID controller. The PID controller is tuned to a bandwidth of 150 Hz with a phase margin of 45 degrees, and it is ensured that the developed reset controllers also have the same phase margin. This is done so that robustness of the system is not compromised.

During literature review it was observed that majority of the research in reset control was focused on the integrator. Reset can be useful in low pass filter of PID, and more importantly in the lead part, as phase advantage from reset is most beneficial in the lead part and can directly help reduce water bed effect. Implementation of reset in the taming pole of

lead component in PID, and in the low pass filter give rise to the following three controller configurations :

- Reset in taming pole for improvement in tracking performance and precision (Controller A)
- Reset in taming pole for improvement in tracking performance and bandwidth (Controller B)
- Reset in low pass filter for improvement in precision (Controller C)

It is shown that the waterbed effect is relaxed using reset control in theory. New design rules are developed for the reset PID controllers. Sufficient conditions for asymptotic stability have been shown to be satisfied. The controllers are then implemented digitally within a MATLAB/Simulink environment and implemented on a dual stage precision system, via a real-time dSPACE DS1103 controller interface.

The improvements in open loop shape shown using describing function can not be definitive proof for improvements in the frequency domain properties of real systems, as the describing function method is only an approximation of the nonlinear controllers. So, closed loop frequency responses were experimentally identified in the practical setup and it was observed that they match well to the frequency responses calculated from describing function analysis. Moreover, in time domain, the performance of the reset controllers are compared in terms of steady state precision with that of the PID controller. The maximum errors in position are shown to be lower with controller A and C. Controller B was tuned to have the same precision as the PID, but with higher bandwidth.

To the fine stage, a fourth order input-shaped reference signal was applied along with second order feedforward. The tracking performances of the reset controllers are studied in comparison to the PID controller as before. The tracking performance is also validated in the dual stage system, by applying a fourth order input-shaped reference signal along with fourth order feedforward. In the dual stage system, the coarse stage is controlled with a PID and the fine stage is controlled with each of the three reset controllers developed. The performance is compared with the results from using PID controllers on both stages and it is observed that as expected, Controller A and Controller C show better tracking performance than PID, while Controller B showed no improvement.

CONTENTS

1

INTRODUCTION

In this section, a basic introduction is given about high precision motion control as commonly practiced in industry , along with the concept of loop shaping and PID control. The factors limiting the maximum achievable performance from PID are discussed. Reset control is introduced as a means of overcoming these limitations. The objective of the thesis is defined, and a brief overview of the thesis is also given.

1.1. HIGH PRECISION MOTION CONTROL

Precision motion control is a very important part of mechatronic systems and has a very wide range of applications. It is of extreme importance in the fields of optical engineering, semiconductor production, and assembly industries for example, where precision in the order of nanometers is required while at the same time achieving high bandwidths. For accurate servo-positioning of mechanical actuators in real life engineering systems, high quality motion control is required to achieve high speeds and precision [1]. Extensive research has been done in this field and many advanced controllers have been developed. Most of these control techniques however, have not been adopted by the industry for various reasons. For example, the state feedback approach and H_∞ control require an accurate model of the system and are very sensitive to parameter variations. As a result, these techniques have mainly stayed in academia. Industrial motion control requires control techniques to be easily adaptable to various applications.

PID control technique is widely applicable and is the easiest to implement. The control scheme is very intuitive and doesn't require complete knowledge of the underlying systems. Tuning PID does not involve extensive numerical computations or complex tools. Robust PID controllers can be tuned using basic rules of thumb. These factors explain why PID control has been the industrial standard for precision motion control.

Loop shaping is an intuitive method used to tune linear PID controllers. It makes use of frequency response functions, which provide a powerful tool to analyze LTI systems through the use of graphic representations such as Bode and Nyquist plots. Knowledge of the poles

and zeros of the system is not necessary, as frequency measurement data can be used to make inferences about performance and stability. Resulting controllers are also generally of low order resulting in easy implementation when using this approach.

Combined with good feed-forward techniques, PID can be used to achieve high speeds and precision and in many cases would be enough to meet the required performance criteria. But in the high - tech industry, design requirements are becoming more and more demanding by the day and hence there is a need to study the limiting factors that prevent us from achieving better performance. Once they are established, possible control solutions that are not bound by these limitations can be applied to improve the performance. Loop shaping technique is introduced first, followed by PID control. For a more detailed text on high precision motion control, the reader can refer to [1].

1.1.1. LOOP SHAPING

Loop shaping is a technique in which the controller is designed in such a way that the frequency response of the open loop transfer function ($L(s) = C(s)P(s)$) has the desired shape in gain and phase. Consider the feedback system shown in Figure 1.1

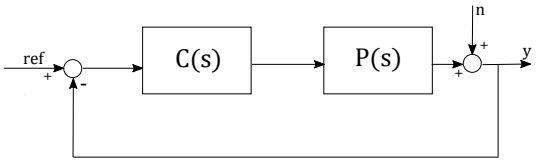

Figure 1.1: Block diagram of closed loop system with controller C(s) and plant P(s)

The concept of loop shaping can be understood through the sensitivity function and complementary sensitivity function of the system. The complementary sensitivity function T(s), defined as the transfer from the reference(ref) to the output(y), describes the ability of the system to act as a servo system, and is given by

$$T(s) = \frac{C(s)P(s)}{1 + C(s)P(s)} \tag{1.1}$$

The sensitivity function S(s) on the other hand is defined as the transfer from noise (n) to the output (y) and describes the ability of the feedback system to reject sensor and any additional noise. It's defined as

$$S(s) = \frac{1}{1 + C(s)P(s)} \tag{1.2}$$

For good reference tracking, the open-loop gain at lower frequencies should be very high ($|L(j\omega)| \to \infty$) such that $\frac{Y(s)}{R(s)} = |T(j\omega)| \approx 1$ and $\frac{Y(s)}{N(s)} = |S(j\omega)| \ll 1$. Similarly at high frequencies the open-loop gain should be low ($|L(j\omega)| \ll 1$) to effectively attenuate noise in the system and hence provide good precision. Around the bandwidth region, the open loop

must have a phase greater than −180° to ensure stability.

Such requirements in the gain and phase behavior guide the control design, as shown in Figure 1.2. Once the open loop is designed, the controller C(s) can be calculated.

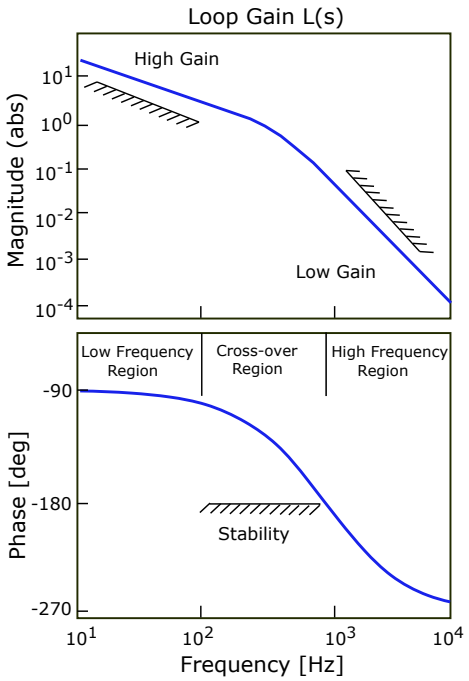

Figure 1.2: Gain and phase behavior to be met through loop shaping. Image courtesy [2]

1.1.2. PID CONTROL

CONTROL THEORY

In a control scheme based on a PID(Proportional-Integral-Derivative) controller, the error signal is computed as the difference between the reference set point and the measured output. This error signal is acted upon by proportional, integrator and derivative terms to obtain the control action.

- The proportional term provides a control signal proportional to the current value of the error and determines how quickly the controller reacts to the error.
- Integrator or lag component accumulates the past values of the error and provides a control signal that tends to bring the error to zero. Hence it plays an important role in the tracking behaviour of the system.
- The derivative or lead component acts on the current rate of change of the error and accounts for future possible errors. It thereby adds a positive phase to the system and is crucial to the stability of the system. A pure differentiating action is physically infeasible as it requires having infinite gain at infinite frequencies. Also, it amplifies the noise at high frequencies. To avoid this, the derivative action is always tamed with a first order LPF.

- Also commonly used in the PID control scheme is an additional low pass filter to attenuate the high frequency noise and higher order dynamics. This low pass filter is instrumental in achieving a high precision.

Transfer function of linear PID in series form is given by:

$$G_{PID} = K_p \underbrace{\left(1+\frac{\omega_i}{s}\right)}_{\text{Lag component}} \underbrace{\left(\frac{s}{\omega_d}+1\right)\Big/\left(\frac{s}{\omega_t}+1\right)}_{\text{Lead component}} \underbrace{\left(\frac{\omega_l}{s+\omega_l}\right)}_{\text{LPF}} \tag{1.3}$$

where ω_I is the frequency at which integral action is stopped, and ω_l is the cut off frequency of the LPF. K_p is the proportional gain. Differentiating action is started at ω_d and tamed at ω_t, and therefore $\omega_t > \omega_c > \omega_d$. The frequency response of PID can be distinguished into 3 parts as can be seen in 1.3

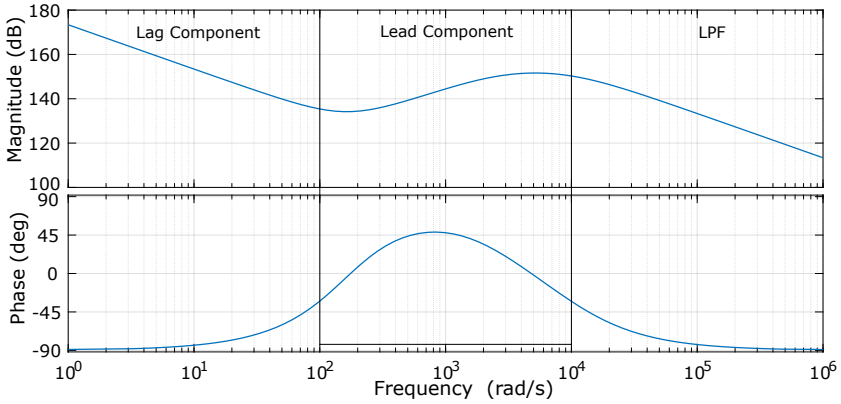

Figure 1.3: Bode plot of PID

PID TUNING THROUGH LOOPSHAPING

To tune the PID controllers, the following basic guidelines are used [2].

1. Positive phase is added to the system in open loop around the bandwidth region to ensure stability, (as explained in 1.1.1) using the differentiator which has a pole at ω_d. In order to add sufficient phase lead to the system, the differentiating action should begin at a frequency one thirds the crossover frequency of the system. This phase addition is accompanied by +1 gain slope. To achieve sufficient phase margin but at the same time have enough attenuation of higher frequencies, the differentiating action should be terminated at a frequency ω_t equal to three times the bandwidth of the system by adding a pole. While this is the rule of thumb, the ratio ω_τ/ω_d can be increased or decreased depending on the phase margin required. Generally the scale ω_c/ω_d is kept equal to ω_τ/ω_c so that maximum phase is added at ω_c.

$$\omega_d = \omega_c/3$$

$$\omega_\tau = 3 \cdot \omega_c$$

2. Integrator increases the low frequency gain through a pole placed at origin and hence provides a favorable loop shape for tracking. Since the integrator creates a 90 degree phase lag, the integrating action should be stopped at a factor 3.33 lower than the frequency at which differentiating action begins to keep the effect of integrators phase lag on the phase margin minimal.
$$\omega_i = \frac{\omega_c}{10}$$

3. The low pass filter decreases the gain at higher frequencies by placing a pole at ω_l. This attenuation in high frequencies provide a better loop shape for precision. In order to keep the phase margin achieved at the crossover frequency intact, the low pass filter should be placed at a frequency 6 to 10 times higher than the bandwidth of the system.
$$\omega_l = (6 \sim 10) * \omega_c$$

4. The open loop gain at the targeted crossover frequency should be equal to one so that the required bandwidth is achieved. The total controller gain (K_t) at the crossover frequency should therefore be chosen equal to the inverse of the gain of the plant at this frequency. As the differentiating action adds gain to the system, the total gain calculated must be divided by three.
$$K_p = \frac{K_t}{3}$$

1.2. LIMITATIONS IN LINEAR CONTROL

PID control has inherent design limitations that no linear control technique can overcome. These limitations can be observed both in time domain and frequency domain. Only select limitations that most affect the performance of linear control systems, with specific focus on PID controllers, are discussed in this section. For a more detailed reference on the fundamental limitations in linear control, [3], and [4] can be referred.

1.2.1. WATER-BED EFFECT

The main limitation in frequency domain is described as the 'Water-bed effect'. For linear systems with no poles in the right half plane, the sensitivity function $S(i\omega)$ has the following property[5]:
$$\int_0^\infty log|S(i\omega)|d\omega = 0 \tag{1.4}$$

In words, the integral of the sensitivity function over the entire frequency range must equal zero. With sensitivity function being the closed loop frequency attenuation from noise to output, it is desirable to have as low a value as possible. But due to water-bed effect it is impossible to decrease sensitivity at all frequencies, because decreasing the sensitivity function at one frequency region would always be accompanied by an increase in sensitivity at

another region in order to maintain the integral at zero. This results in a trade off between competing performance criteria. For example, increasing the bandwidth to improve the disturbance rejection at lower frequencies would increase the gain at higher frequencies thereby affecting the noise attenuation at those frequencies.

1.2.2. BODE'S GAIN PHASE RELATIONSHIP

The limitations in frequency domain can also be illustrated using Bode's gain phase relationship. For a minimum phase stable system $G(s)$, it can be derived that[5]

$$\angle(G(i\omega_0)) \approx \frac{\pi}{2}\frac{dlog|G(i\omega_0)|}{dlog\omega} \tag{1.5}$$

According to (1.4), for a linear system, the relationship between the gain and the phase of the system is constant. Gain slopes of +20 dB/dec and -20 dB/dec would be accompanied by 90 degree phase lead and lag respectively. Due to this limitation, using an integrator to improve the tracking would cause a phase lag affecting the stability. Derivative term can be used to provide a phase lead, but that would amplify the high frequency noise . Using a low pass filter to achieve high frequency roll off would again reduce the phase at the crossover frequency. Such unavoidable trade-offs limit the maximum bandwidth and precision that can be achieved using a PID, or any linear control technique for that matter.

1.3. PROBLEM STATEMENT

PID control being a linear control technique, has been shown to have inherent design limitations that constrain the maximum possible performance that can be achieved in the system, in terms of tracking, robustness, and/or precision. These limitations occur in the form of unavoidable trade offs that force a compromise in one or more performance criteria when another criterion needs to be improved.

1.4. OVERCOMING FUNDAMENTAL LIMITATIONS

It has been established that it is necessary to look into nonlinear control techniques to reduce the water bed effect and break the gain phase relationship barrier. While choosing a non linear control solution, the following conditions should be satisfied. The control technique:

- should not be bound by Bode's gain phase relationship
- should be compatible with PID control scheme
- should be easily implementable and adaptable to wide range of systems
- should not require thorough prior knowledge of the system for design

Reset control is a nonlinear technique that is becoming increasingly popular, in which a linear controller is provided with a mechanism to reset all or a subset of its states when a specified condition holds. In the most common approach to reset, the states are reset to zero or to a fraction of the before reset value, when the error crosses zero. However, many variations are possible.

Literature is available that show that reset control is not bound by Bodes gain phase relationship and that the adversity of waterbed effect is reduced. For instance, in [6], reset control has been used to meet desired control specifications even in plants with large parameter uncertainty. Reset has been used to improve mid-frequency disturbance rejection in hard disk systems [7]. In [8], a fractional order reset integrator is used to improve performance in servomotors. In [9], it is shown that reset can be used to reduce overshoot in plants that have an integrator. Inspite of the potential shown by reset, it is observed that much of the research in reset control was focused on the integrator. There have been efforts in investigating other reset elements as well. For example, in [10], a phase lead reset compensator has been used to increase phase margin. In [11], a first order reset element was used to reduce overshoot and settling time in second order systems. A generalized fractional order reset element was introduced in [12]. However apart from reset integrator, the use of reset elements within the framework of PID for improved performance has not been well investigated.

1.5. OBJECTIVE

The objective the thesis can be defined as,

To develop theory and guidelines for Reset PID control, and validate in a fast, high precision setup.

The sub-ojectives can be organised as follows:

- Develop theory for implementation of reset in PID to obtain best possible performance.
- Devlop guidelines for tuning reset PID, that ensure stability and given specifications.
- Implement the developed controllers in a practical setup and validate improvements in bandwidth and precision.
- Create a toolbox for auto tuning of controllers.

1.6. OUTLINE

The thesis report is structured as follows : Reset control and the current state of the art in the field is discussed in *Chapter 2 : Reset Control*. In *Chapter 3: Reset in PID*: the theory behind using reset in PID control to achieve improvements in bandwidth and preci-

sion. In *Chapter 4 : System Overview*, the dual stage mechanical setup used for validation is presented. Development of reset controllers for the precision stage, along with implementation methods are discussed in *Chapter 5 : Controller Design*. The methods used for validation in the fine stage and the results in both time domain and frequency domain are given in *Chapter 6 : Experimental Verification*. The tracking performance of the dual stage system is investigated in *Chapter 7 :Experimental results - Dual stage*. Following this, in *Chapter 8 - Tuning Reset PID*, basic guidelines for tuning reset PID controllers are provided. Finally, general conclusions along with recommendations for further research are given in *Chapter 9 : Conclusions*.

2

RESET CONTROL

In this chapter, an introduction to reset control is given. A method for analyzing reset controllers, namely describing functions, is discussed. This is followed by a brief overview of various reset elements developed so far in academia. There are other types of reset controllers than those discussed here, like reset systems that reset at fixed time intervals, and those that reset at the surfaces of a predefined reset band. But focus has been kept on the most widely used form of reset control, based on zero crossings of the error, because sufficient literature and tools are available for checking stability and analysis in the frequency domain. A method for tuning nonlinearity in the system is explained, followed by stability conditions that need to be satisfied by reset controllers.

2.1. GENERAL FORM OF RESET CONTROLLER

A general form of reset controller would require two inputs in addition to the error signal $e(t)$ required by the regular controller, as shown in 2.1b. One input $c(t)$ would specify the reset instants. Thus, at the moments at which c(t) satisfies the specified reset condition, for example, zero crossings of $c(t)$, the states are reset. The after reset value is specified by the third input $a(t)$.

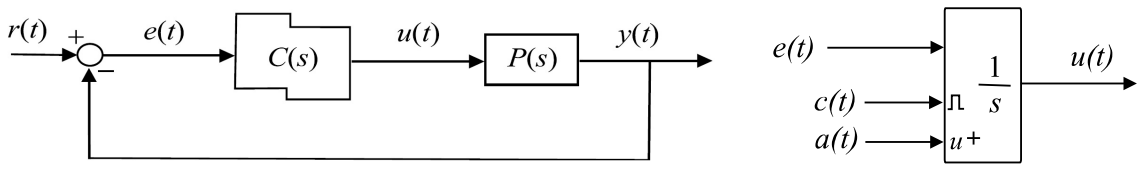

(a) (b)

Figure 2.1: (a) Feedback loop with reset controller C(s) and plant P(s). (b) Basic reset integrator with two additonal inputs. Image courtesy [5]

Consider the feedback loop shown in Fig. 2.1a. The reset element C(s) which has linear base dynamics that resets at zero crossings of e(t) can be described as follows:

$$\begin{aligned} \dot{x}(t) &= A_r x_r(t) + B_r e(t) && when\ e(t) \neq 0 \\ x(t^+) &= A_\rho x_r(t) && when\ e(t) = 0 \\ u(t) &= C_r x_r(t) + D_r e(t) \end{aligned} \tag{2.1}$$

where $x(0) = x_0$; $x(t^+) \triangleq \lim_{s \to t+0} x(s)$.

A_r, B_r, C_r, D_r represent the state space matrices of the base linear system. $e(t)$ is the error signal that is input to the reset controller and u(t) is the controller output . $x_r(t) \in \mathbb{R}^n$ is the state vector. The first and third equation denote the continuous or flow mode that hold true whenever the reset condition is not met. At the reset instants, the jump mode is triggered, given by the second equation. A_ρ is a diagonal matrix that determines the values to which the states are to be reset.

2.2. ANALYSIS OF RESET CONTROL SYSTEMS

The FRF methods discussed in 1.1.1 is not readily applicable to reset control as it is a nonlinear technique. There are many methods to analyze nonlinear control problems. Describing function (DF) method is one such technique, which is an extension of the frequency response method and also inherits some of its desirable properties, and can be used to study the frequency domain characteristics of non linear elements. Through quasi-linearization of the non linear element, the DF method helps extend the concept of FRF to non linear systems. This method makes the assumption that non linear system behavior has a quasi-linear amplitude dependent relation between sinusoidal excitation inputs and the steady state response at the fundamental excitation frequency. This approximation is possible when the system under consideration has low pass characteristics that filters out the higher harmonics. Since the relation is amplitude dependent, the excitation amplitude needs to be considered as a parameter.

For a sinusoidal input function given by

$$a \sin(\omega t) \tag{2.2}$$

the first harmonic of the output that is assumed to sufficiently approximate the response is given by

$$Z_1(t) = g_{re} \sin(\omega t) + g_{im} \cos(\omega t) \tag{2.3}$$

The describing function of the nonlinear system is defined as the "complex ratio of the fundamental harmonic component of the output to the input", i.e.

$$\eta(a, \omega) = \frac{g_{re} + j g_{im}}{a} \tag{2.4}$$

In the next section, it will be shown through the use of describing functions, that reset systems show better phase behaviour compared to linear controllers while having comparable

gain characteristics. A more detailed discussion on describing functions can be found in [13]. It must be noted that describing functions can not completely describe a system and can only be used as an approximation.

2.3. RESET ELEMENTS

2.3.1. CLEGG INTEGRATOR

Reset controllers were first proposed by J.C Clegg in 1958[14]. The Clegg integrator was designed to serve as an alternative to conventional linear integrator, which is very essential in motion control. Each integrator in a system causes a phase lag of 90 degrees, as shown by Bodes gain - phase relationship. This imposes severe limitations when trying to meet phase margin and overshoot requirements. A Clegg integrator is shown to have superior performance than a linear integrator.

A Clegg integrator has an integrator as the base linear system and it integrates the error signal. The reset instants are the zero crossings of the error signal, at which moments the output is reset to zero. It is a specific case of the reset controller defined in (2.1), and can be described as follows:

$$\begin{aligned} \dot{u}(t) &= e(t) && when\ e(t) \neq 0 \\ u(t^+) &= 0 && when\ e(t) = 0 \end{aligned}$$

with $u(0) = u_0$. Fig.2.2b shows the response of the linear and Clegg integrator to a sinusoidal e(t).

The describing function of a Clegg integrator is given by :

$$CI(j\omega) := \frac{1.62e^{-j30^\circ}}{j\omega} e^{j52^\circ} \tag{2.5}$$

thus indicating a 52° positive phase compared to a linear integrator. The gain is 1.62 times higher than that of the integrator. However, the slope of gain is same as that of linear integrator. The frequency response of the Clegg integrator is compared with that of a linear integrator in 2.2a

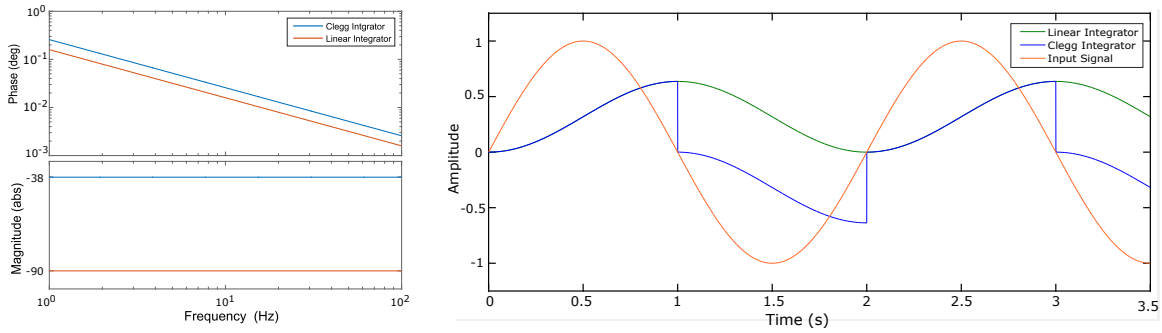

(a) (b)

Figure 2.2: (a) Frequency response comparison between linear and Clegg Integrator. (b) Response of Clegg and Linear Integrator to sinusoidal input

2.3.2. FIRST ORDER RESET ELEMENT

The First Order Reset Element(FORE) was first introduced in [6], and can be seen as a generalisation of the Clegg Integrator. The base linear system has a first order lag filter characteristic and is given by

$$C(s) = \frac{K}{s+a}$$

The output of the FORE also resets to zero at zero crossings of the input. FORE can be described by

$$\dot{u}(t) = -au(t) + Ke(t) \qquad when\ e(t) \neq 0$$
$$u(t^+) = 0 \qquad when\ e(t) = 0$$

Upto the corner frequency, the behavior of the FORE is similar to that of linear lag filter as shown in 2.3b. The phase lead achieved by FORE compared to linear filter at higher frequencies is the same as that for a Clegg integrator. It can also be seen that the cutoff frequency is altered by a small margin by resetting.

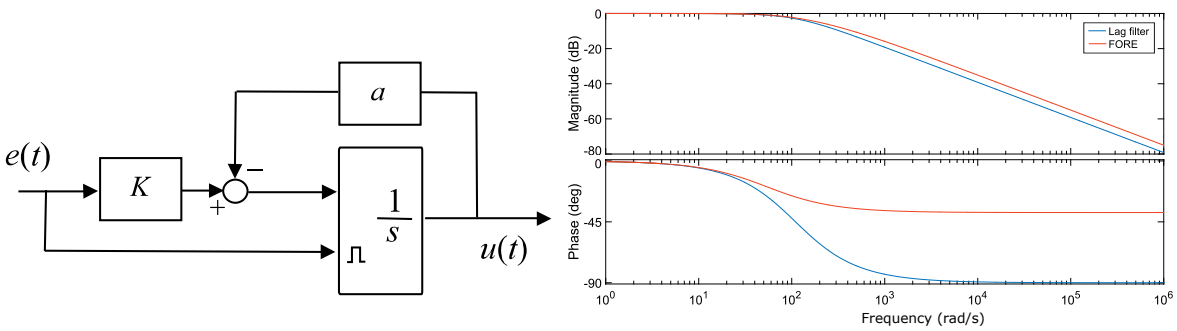

(a) (b)

Figure 2.3: (a) Block diagram of FORE. Image courtesy [5]. (b) Frequency response of FORE compared with that of a lag filter and a Clegg integrator

2.3.3. SECOND ORDER RESET ELEMENT

Second Order Reset Elements (SORE) were designed, with the main motivation being the importance of second order filters such as notch filter and low pass filter in the field of motion control [15]. SORE provides more design freedom and better phase properties than a FORE.

A second order low pass filter is given by

$$C(s) = \frac{\omega_p^2}{s^2 + 2\beta_p\omega_p s + \omega_p^2}$$

where ω_p is the corner frequency. A SORE with low pass filter as the base dynamics can be described by the following parameters for (2.1).

$$A_r = \begin{bmatrix} 0 & 1 \\ -\omega_p^2 & -2\omega_p\beta_p \end{bmatrix} \qquad B_r = \begin{bmatrix} 0 \\ \omega_p^2 \end{bmatrix}$$
$$C_r = \begin{bmatrix} 1 & 0 \end{bmatrix} \qquad A_\rho = \begin{bmatrix} 0 & 0 \\ 0 & 0 \end{bmatrix} \tag{2.6}$$

In this case, both the states of the controller are reset to zero and it is termed full reset. The parameter β is the damping coefficient, which can be used to tune the sharpness of the filter around the corner frequency.

2.4. CONTROLLING NONLINEARITY

The reset matrix A_ρ in (2.1) provides an additional degree of freedom in tuning the system and is defined γI_n where n is the number of states in the system.

If the resetting parameter $\gamma = 1$, the reset element reduces to its base linear system as no reset occurs and $\gamma = -1$ denotes extreme reset. As $|\gamma - 1|$ increases, the nonlinearity in the system increases because the magnitude of jump in state value increases. Increase in nonlinearity is not desired due to the associated higher order dynamics. The variation of phase lag with change in γ is shown in Fig. 2.4a, and it can be seen that the more nonlinear the system is, greater is the phase benefit.

Cutoff frequency of GFORE also varies with change in γ . The ratio of cutoff frequency of reset filter to that of lag filter (β) is plotted in Fig. 2.4b for different values of γ . Choosing γ values between -1 and 1 can help attain the desired trade-off between phase lag, cutoff frequency and non linearity and hence can be used a tuning parameter in design of reset controllers.

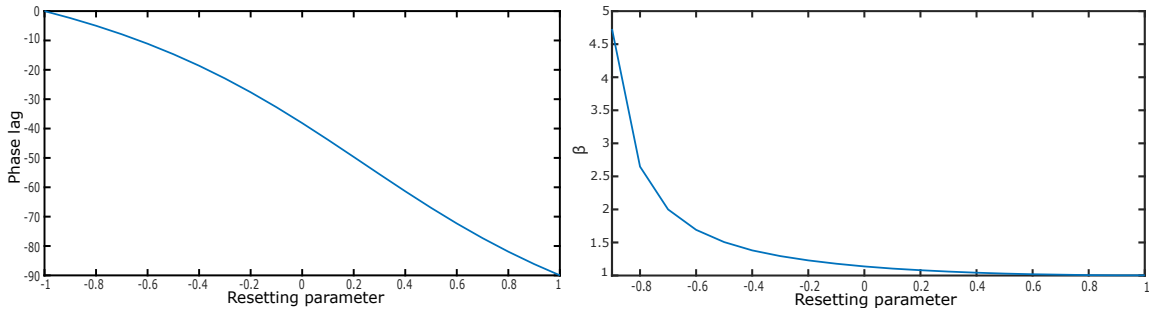

(a) (b)

Figure 2.4: (a) Variation of phase lag with change in γ. (b)Variation of ratio β with change in γ.

2.5. STABILITY OF RESET CONTROL SYSTEMS

2.5.1. GLOBAL ASYMPTOTIC STABILITY

The asymptotic stability conditions to be satisfied for a general reset system is developed in [7] and is briefly discussed here. These criteria are used to verify the stability of the reset controllers developed.

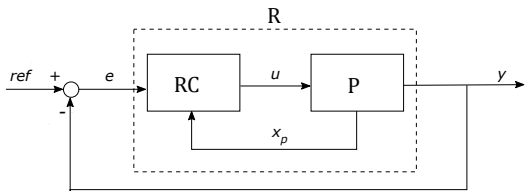

Figure 2.5: Control Architecture

Consider the feedback loop shown in Figure 2.5, with plant P and controller RC described as follows:

$$P = \begin{cases} \dot{x_p} = A_p x_p + B_p u \\ y = C_p x_p \end{cases} \tag{2.7}$$

$$RC = \begin{cases} \dot{z} = A_r z + A_{rp} x_p + B_r e, & e \neq 0 \\ z(t^+) = A_\rho z + A_{\rho p} x_p, & e = 0 \\ u = C_r z + C_{rp} x_p + D_r e \end{cases} \tag{2.8}$$

where, $z \in \Re^r$ and $x_p \in \Re^p$.

Combining P and RC, the combined state space of the open loop reset system R can be represented as

$$R = \begin{cases} \dot{x} = Ax + Be, & e \neq 0 \\ x(t^+) = \sigma_\rho x, & e = 0 \\ y = Cx \end{cases} \tag{2.9}$$

where x is the state vector of R, and

$$A = \begin{bmatrix} A_p + B_p C_{rp} & B_p C_r \\ A_{rp} & A_r \end{bmatrix}, \; B = \begin{bmatrix} B_p D_r \\ B_r \end{bmatrix}$$
$$C = \begin{bmatrix} B_p D_r \\ B_r \end{bmatrix}; \sigma_\rho = \begin{bmatrix} I & 0 \\ A_{\rho p} & A_\rho \end{bmatrix}$$

For ease of representation following notations are defined:

$$\Lambda(\omega) \triangleq \omega^2 I + A^2$$
$$\triangle(\omega) \triangleq I + e^{\frac{\pi}{\omega}A}$$
$$\triangle_\rho(\omega) \triangleq I + \sigma_\rho e^{\frac{\pi}{\omega}A}$$
$$\Gamma_\rho(\omega) \equiv \triangle_\rho^{-1}(\omega)\sigma_\rho\triangle(\omega)\Lambda(\omega)^{-1}$$
$$\Omega = \{\omega > 0 | \pm j\omega \text{ are eigen values of A}\}$$
$$\Omega_\rho = \{\omega > 0 | \lambda(\sigma_\rho e^{\frac{\pi}{\omega}A})| < 1\}$$

Consider the sinusoidal excitation input

$$e(t) = \alpha \sin(\omega t)$$

The time instants(t_k) at which reset occurs is given by

$$t_k = k\pi/\omega \quad k = 0, 1, ..$$

Defining,

$\eta_k = x(t_{2k}^+)$, $\zeta_k = x(t_{2k+1}^+)$ and $\psi(t) \triangleq \int_0^t e^{-As} B \sin(\omega s) ds$

the solution of the augmented plant with initial condition $x(0^+) = \eta_0$ has been shown to be

$$x(t) = \begin{cases} e^{A(t-t_{2k})}\eta_k + \alpha e^{At}[\psi(t) - \psi(t_{2k})], & t \in (t_{2k},\ t_{2k+1}] \\ e^{A(t-t_{2k+1})}\zeta_k + \alpha e^{At}[\psi(t) - \psi(t_{2k+1})], & t \in (t_{2k+1},\ t_{2k+2}] \end{cases} \tag{2.10}$$

where,

$$\begin{aligned} \zeta_k &= \sigma_\rho e^{\frac{\pi}{\omega}A}[\eta_k + \alpha\psi(\tfrac{\pi}{\omega})], \\ \eta_k + 1 &= \sigma_\rho e^{\frac{\pi}{\omega}A}[\zeta_k - \alpha\psi(\tfrac{\pi}{\omega})],\ \eta_0 = x(0^+) \end{aligned} \tag{2.11}$$

For the solution given in Equation 2.10 to be stable, the parameters ζ_k and η_k given in Equation 2.11 should converge as $k \to \infty$, leading to the stability condition

$$|\lambda(\sigma_\rho e^{\frac{\pi}{\omega}A})| < 1 \tag{2.12}$$

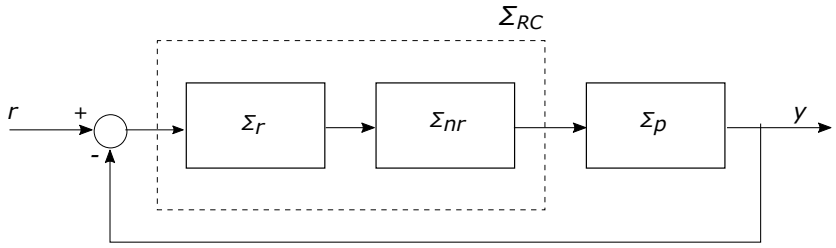

Figure 2.6: Block diagram of reset controller Σ_{RC} in closed loop with plant Σ_p.

ζ_k and η_k converge if and only if Equation 2.12 is satisfied. Furthermore, the sinusoidal input describing function of system in Equation 2.8 was derived as the ratio of the laplace transforms of the steady state output (Y_{ss}) and the input(E), and is given below.

$$G(j\omega) = \frac{Y_{ss}}{E} = C_r^T (j\omega - A_r)^{-1}(I + j\Theta_\rho(\omega))B_r \tag{2.13}$$

where,

$$\Theta_\rho = \Delta - \frac{2\omega^2}{\pi}\Delta(\omega)[\Gamma_\rho(\omega) - \Lambda^{-1}(\omega)] \tag{2.14}$$

2.5.2. LYAPUNOV STABILITY

Consider reset system Σ_{RC} in closed loop with a plant Σ_P as shown in Figure 2.6. The controller Σ_{RC} is separated into a part Σ_r whose states are reset and a part Σ_{nr} whose states are not reset. For such a system,asymptotic stability is guaranteed when following conditions are true:

Theorem [5] *Let $V : \mathbb{R}^n \to \mathbb{R}^n$ be a continuously differentiable, positive-definite, radially unbounded function such that*

$$\dot{V}(x) := \left(\frac{\partial V}{\partial x}\right)^T A_{cl}x < 0, \text{ if } e(t) \neq 0, \tag{2.15}$$

$$\Delta V(x) := V\left(A_\rho^x\right) - V(x) \leq 0, \text{ if } e(t) = 0 \tag{2.16}$$

where A_ρ is the reset matrix defined as

$$A_\rho^* = \text{diag}(A_\rho,\ I_{n_{nr}},\ I_{n_p}) \tag{2.17}$$

where n_{nr} is number of states of Σ_{nr} and *n_p is the number of states in Σ_p*

A_{cl} is the closed-loop A-matrix:

$$A_{cl} = \begin{bmatrix} A_r & B_r C_{nrp} \\ -B_{nrp}C_r & A_{nrp} \end{bmatrix} \tag{2.18}$$

in which (A_r, B_r, C_r, D_r) *are the state space matrices of* Σ_r *and* $(A_{nrp}, B_{nrp}, C_{nrp}, D_{nrp})$ *are the state space matrices of* Σ_{nr} *and* Σ_p *in series.*

Then the reset control system is asymptotically stable.

For quadratic stability of the system, the conditions (2.15), and (2.16) must hold true for a potential function $V(x) = x^T P x$ with $P > \mathrm{O}$. Based on this, the following theorem was developed for proving quadratic stability.

Theorem [5] *There exists a constant* $\beta \in \mathbb{R}^{n_r \times 1}$ *and* $P_\rho \in \mathbb{R}^{n_r \times n_r}, P_\rho > 0$ *where* n_r *is the number of reset states, such that the restricted Lyapunov equation*

$$P > 0,\ A_{cl}^T P + P A_{cl} < 0 \tag{2.19}$$

$$B_0^T P = C_0 \tag{2.20}$$

has a solution for P*, where* C_0 *and* B_0 *are defined by*:

$$C_0 = \begin{bmatrix} \beta C_{nrp} & 0_{n_r \times n_{nr}} & P_\rho \end{bmatrix} \tag{2.21}$$

$$B_0 = \begin{bmatrix} 0_{n_{nrp} \times n_r} \\ 0_{n_r \times n_r} \\ I_{n_r} \end{bmatrix} \tag{2.22}$$

Both conditions have been used to test stability of all developed controllers.

3

RESET IN PID

In this chapter, the theory behind the application of reset in the PID control loop is detailed. It was discussed in section 1.4 that there has been lack of research on reset control within PID framework, especially on elements other than integrator. Therefore, implementation of reset in the other two memory elements within the PID structure, namely the taming pole of the lead component and low pass filter is explored with focus on improving bandwidth and precision. Through describing function analysis, the developed controllers are compared with linear PID.

3.1. RESET IN TAMED PART OF LEAD COMPONENT

As discussed in section subsection 1.1.2, differentiator or lead component of the PID adds essential phase to the system in bandwidth region to achieve stability and robustness. Phase at the crossover frequency also affects the maximum overshoot of the system. Differentiator is tamed by placing a pole at ω_t because having large gains at higher frequencies is not desirable for noise attenuation and precision. The maximum phase lead that can be achieved from the differentiator in the absence of this taming pole would be 90°. However, the pole reduces the maximum phase lead to a value which depends on frequency interval between the zero and the pole. By symmetrically placing the zero and pole around the crossover frequency ω_c, it is ensured that the maximum phase from lead is achieved at bandwidth. Fig. 3.1a shows the frequency response of a typical differentiator used in PID.

Higher and lower phase margins can be achieved by increasing or decreasing the frequency range between ω_d and ω_t respectively. The problem with this approach is that it results in a trade-off between tracking and precision performance on one side and stability and robustness on the other. This can be observed in Fig. 3.1b. As the positive phase obtained increases with increase in the ratio of ω_t to ω_d, the gain at higher frequencies is also increased, which affects the precision of the system. As a result, with the linear design, it is not possible to improve precision while having the same degree of robustness. Also, with increasing phase, there is a decrease in low frequency gain thereby affecting tracking behavior.

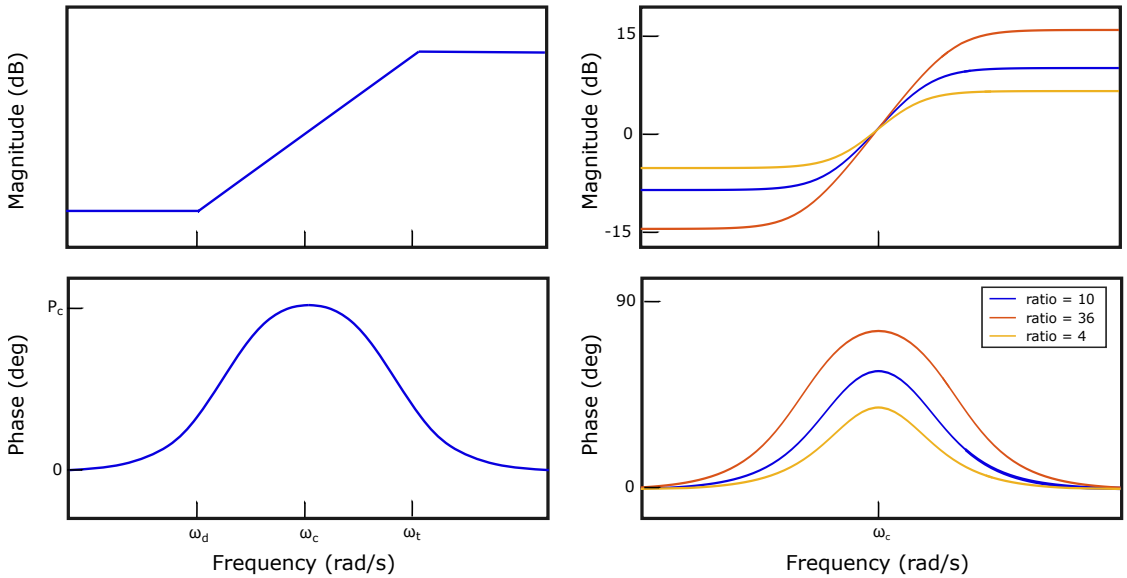

Figure 3.1: (a) Bode plot of a differentiator. (b) Bode plot showing increase in maximum phase and also high freqeuncy gain with increasing ratio of ω_t to ω_d

Reset can be introduced in this tamed differentiator to improve performance such that this fundamental limitation is overcome. Reset is introduced such that only the taming pole is reset resulting in the reset and non-reset parts (as introduced in section 2.5.2) given by:

$$\Sigma_{nr} = \left(\frac{s}{\omega_d} + 1\right); \quad \Sigma_r = \frac{1}{\left(\frac{s}{\omega_t} + 1\right)} \tag{3.1}$$

Although the non-resetting part as given in (3.1) is not a proper function, the completed non-resetting part of Reset PID also consists of integrator and LPFs and hence will be proper. In the case that this is not true, an LPF can be added at a frequency where it does not affect phase at bandwidth, purely to make the function proper.

The frequency response obtained through describing function analysis is compared with that of a linear tamed differentiator in Fig. 3.2a. It can be seen that for a similar gain behavior, phase at frequencies higher than ω_t is not zero in the case of reset. If $\gamma = 0$ is used, the positive phase achieved would be 52 degrees.

It can be seen that phase from resetting is mainly added at higher frequencies beyond the bandwidth and hence it is not useful. However, ω_t can be brought closer to ω_d and can even be made equal to ω_d to obtain a 0 dB gain line with a positive phase, as shown in Fig. 3.2. Thus, phase addition at bandwidth is done purely through reset and not differentiating action. To compensate for changes in cutoff frequency due to reset (as shown in Fig. 2.4b), a factor α is used. The reset element can be reformulated as given in (3.2).Since γ determines

amount of phase lead achieved, this is chosen to ensure that the same amount of phase is added as with the originally designed differentiator.

$$\Sigma_r = \frac{1}{\left(\frac{s}{\alpha\omega_d} + 1\right)} \tag{3.2}$$

It can be observed that the gain at high frequency is lower than the PID, while the low frequency gain is increased, without affecting the phase margin. It can be concluded that theoretically, better tracking and better precision has been achieved while maintaining the same robustness, which was impossible to do with linear control.

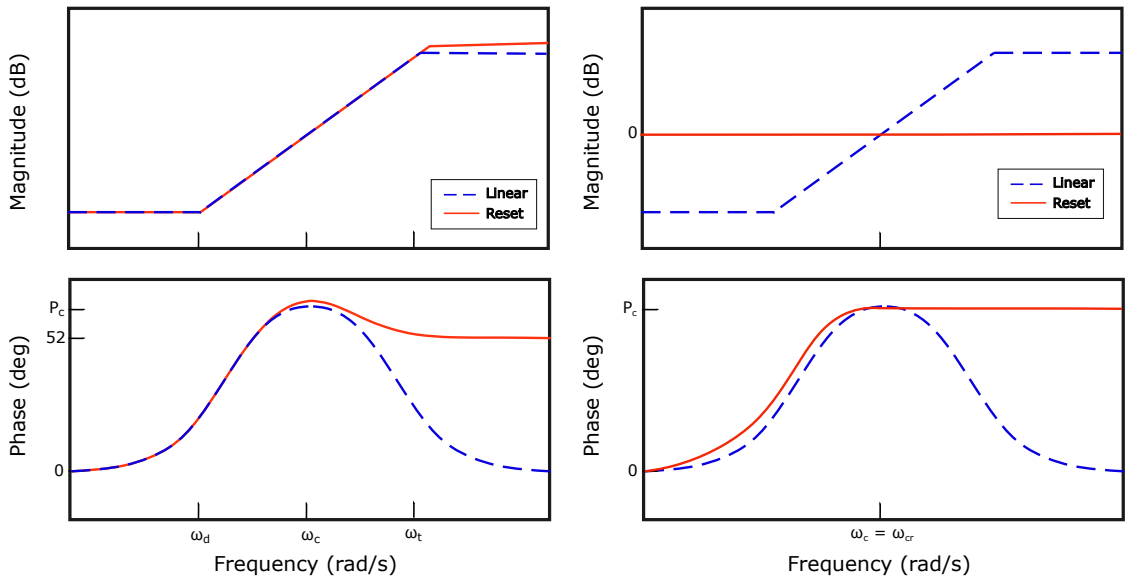

Figure 3.2: (a)Describing function analysis shows positive phase added by reset at frequencies above ω_t when compared to a linear lead component. (b) Reset can be used to achieve the same phase lead with favourable gain behavior.

The reset element, when combined with an integrator and low pass filter, forms Reset PID controller A, given by (3.3).

$$\Sigma_{RC} = \underbrace{\left(\frac{\alpha\omega_d}{s+\alpha\omega_d}\right)}_{\Sigma_r} \underbrace{K_p\left(1+\frac{\omega_i}{s}\right)\left(1+\frac{s}{\omega_d}\right)\left(\frac{\omega_l}{s+\omega_l}\right)}_{\Sigma_{nr}} \tag{3.3}$$

K_p is chosen such that the open loop gain calculated from describing function analysis equals unity at ω_c . The other terms in (3.3) are chosen per guidelines given in subsection 1.1.2.

By increasing the controller gain such that the gain at high frequencies equals that of PID, an increase in bandwidth can be achieved for the same phase margin and precision as

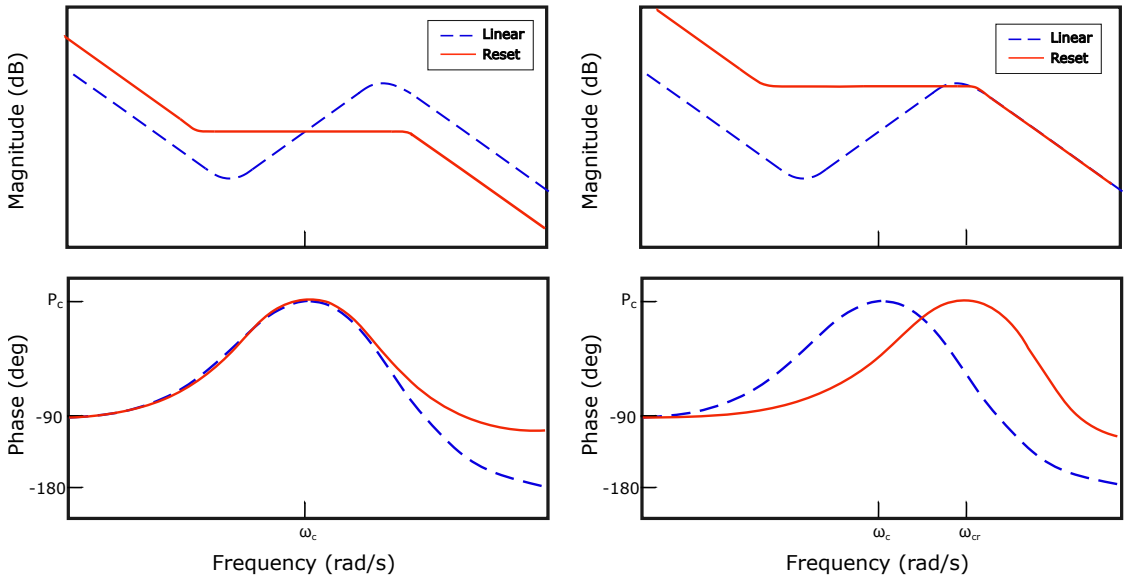

Figure 3.3: (a) Comparison of describing function of Reset PID controller A with a PID controller having the same bandwidth and phase margin. (b) Comparison of describing function of Reset PID controller B with a PID controller having the same precision and phase margin.

shown in 3.3b. It can be seen that bandwidth has increased from ω_c to ω_{cr}. This controller, which provides improved tracking and bandwidth for the same phase margin and precision, will be referred to as Reset PID Controller B. Gain for Controller B at low frequencies is higher than that of Controller A, thereby indicating a further improvement in tracking performance.

3.2. RESET IN LPF

As discussed in section subsection 1.1.2, a low pass filter is commonly used in PID as it is desirable to decrease the open loop gain at high frequencies as quickly as possible. This is done to reduce the complementary sensitivity at high frequencies and thereby improve noise attenuation. Phase lags caused by LPF at frequencies below cutoff frequency can affect the phase around the bandwidth of the system. This causes a tradeoff between robustness and precision and therefore there is a limitation on the order of the LPF that can be used and on how close to bandwidth the LPF can be placed.

When reset is implemented in the LPF, there is a reduction in the maximum phase lag of the filter and also on how fast the phase decreases. Frequency response of a reset LPF and its corresponding linear LPF are compared in 3.4a. It can be seen that for an LPF with corner frequency at ω_l, the reset filter shows lesser phase lag at bandwidth ω_c than the linear filter. This phase advantage can be used to place the reset LPF at a lower frequency (ω_{lr}) than linear LPF, which provides better attenuation of high frequencies, as shown in 3.4b. It can be seen that the corner frequency of LPF is reduced by a factor $\nu = \omega_l/\omega_{lr}$, without affecting the phase at bandwidth.

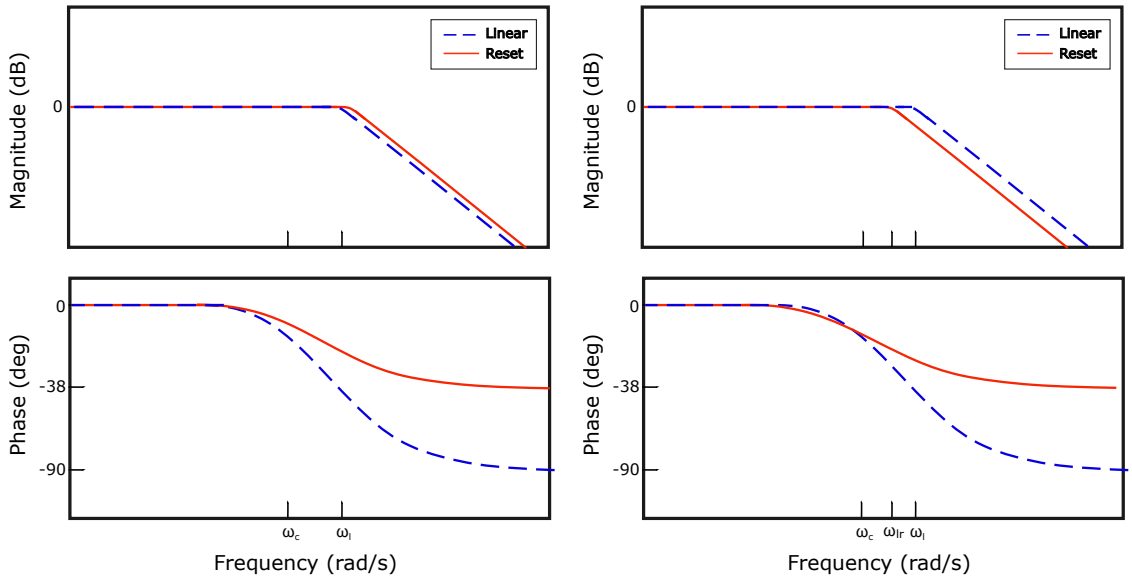

Figure 3.4: (a) Comparison of describing function of Reset LPF with a linear LPF having the same corner frequency (b) Corner frequency of Reset LPF is reduced so that phase at ω_c is equal to that of linear LPF.

It must be noted that the cutoff frequency of the filter increases due to reset, as explained in section 2.4. This reduces the factor ν and the improvement in attenuation that can be achieved. Due to this tradeoff between phase lag and cutoff frequency, γ value is fixed at 0 for reset LPF.

Apart from describing function analysis, the improvement in noise attenuation especially from the point of precision can even be seen in time domain also. Due to the chosen γ value, output of the filter is reset to zero at zero crossings of input signals as shown in 3.5a. The number of resets increases as signal frequency increases and this results in the reset LPF letting through much less high frequency signal than a linear LPF. Necessary condition is that the signal has zero mean and doesn't contain significant low frequency signals. It must be noted that the low pass characteristic of the filter is preserved because between reset instants, reset filter shows linear behavior. Therefore, when there is no tracking signal present, reset LPF can provide better precision even when describing functions show no reduction in high frequency gain. This is verified by applying a multisine signal with randomized phase as input to a linear and reset LPF with equal corner frequencies and comparing the outputs in open loop. This is shown in 3.5b. The RMS value of output of reset LPF is reduced by around 70 % compared to linear LPF.

Reset LPF, when combined with an integrator and lead component, forms Reset PID controller C given by

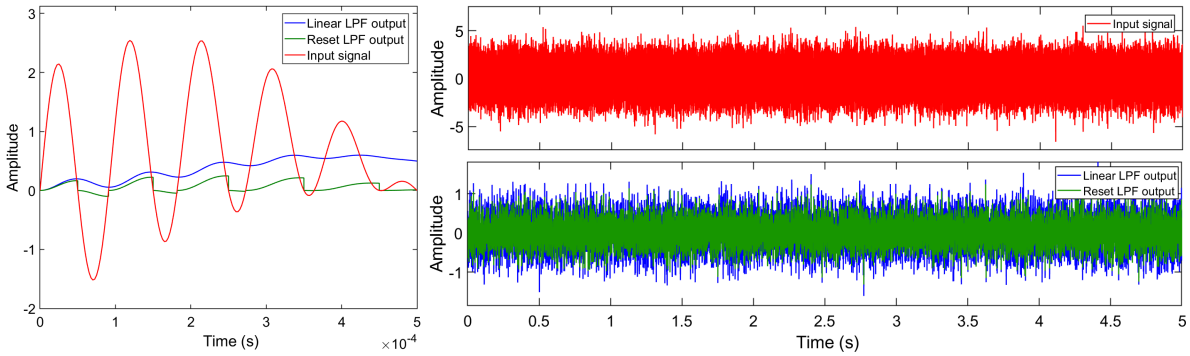

(a) (b)

Figure 3.5: (a) Output of reset LPF is reset to zero at zero crossings of signal with high frequency content. (b) Comparison of output of Reset LPF and linear LPF for multisine input signal.

$$\Sigma_{RC} = \underbrace{\left(\frac{\omega_{lr}}{s+\omega_{lr}}\right)}_{\Sigma_r} \underbrace{K_p\left(1+\frac{\omega_i}{s}\right)\left(1+\frac{s}{\omega_d}\right)\Big/\left(\frac{s}{\omega_t}+1\right)}_{\Sigma_{nr}} \tag{3.4}$$

where ω_{lr} denotes the corner frequency of reset LPF.

4

System Overview

In this chapter, the experimental setup, a dual stage positioning system is described. Following a brief overview of the software and hardware, the two stages of the sytem are discussed in more detail. In the next section, the process of system identification and parameter estimation is detailed.

4.1. Experimental Setup

The setup used in this thesis to validate the performance is a high precision one degree of freedom dual stage positioning system, which was fabricated in 2016 by a former student B.J. Joziasse, at the department PME[16]. The setup was modified to better suit the demonstration of the developed control technique.

The demonstrator consists of a coarse stage and a fine stage, both of which can be actuated separately. The coarse stage is a commercially available 1 DOF positioning system, with a built in linear encoder. The stator of the fine stage is mounted on top of the coarse stage mover. A Lorentz actuator is used to actuate the fine stage. The coil of the Lorentz actuator is attached to the stator and the permanent magnets are mounted on the mover. Parallel leaf flexures are used for the linear guiding of the fine stage. The position of the fine stage is measured using a laser interferometer. The conceptual drawing is shown in Figure 4.1

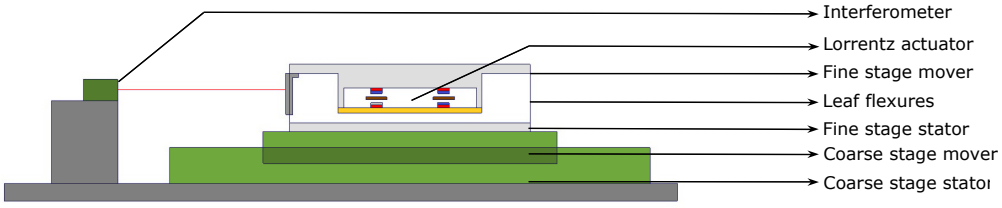

Figure 4.1: Conceptual system drawing

A dSPACE DS1103 real time control system acts as the interface between the computers and the plant. Controllers developed using MATLAB/Simulink environment are run real time

in dSPACE. This combination of hardware and software allows quick prototyping and tuning. The dSAPCE reads out position measurements of both the stages and also applies the required voltage signals computed by the controllers to the system. For the analog signals in the system, 16 bit A/D and D/A converters are used. The digital phase quadrature signals of the position measurements are read out using a 24 bit encoder interface. Additional communication signals required for the Aerotech Soloist motion controller are provided via digital I/O. The controller runs at a cycling frequency of 10 kHz.

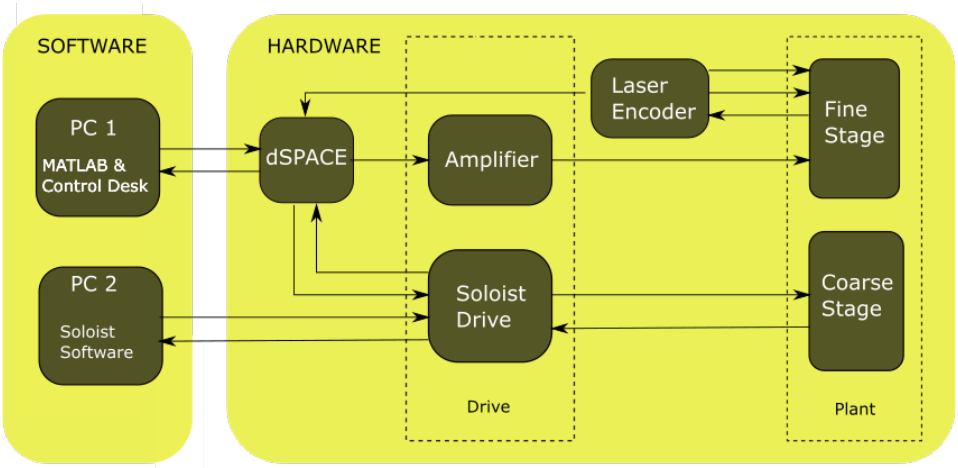

Figure 4.2: System overview

4.1.1. COARSE STAGE

A (*Aerotech ABL10100LT*) 1 DoF stage shown in 4.3a was used for the coarse stage. The stage comprises of an air bearing guide with a stroke of 100 mm, a linear motor for actuation. The specifications of the stage and further details can be found in Appendix A.1.

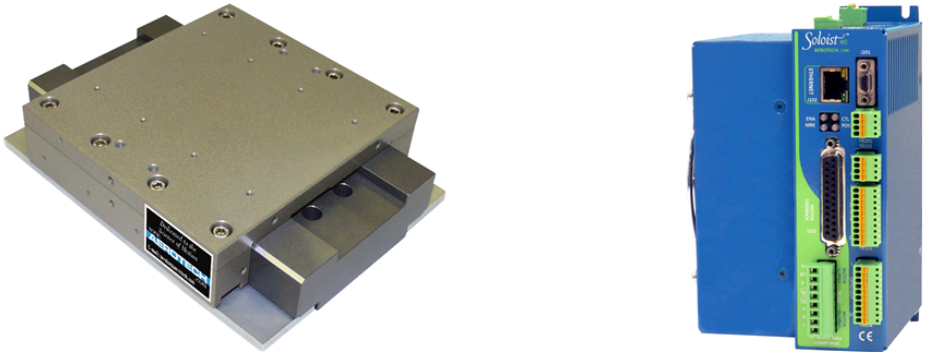

(a) Aerotech ABL10100LT (b) Aerotech Soloist ML

Figure 4.3: An Aerotech ABL10100LT linear stage is used as a coarse stage. The stage is driven by an Aerotech Soloist ML.

The linear stage is driven using an *Aerotech Soloist ML*, shown in 4.3b. It comprises of a power supply, amplifier and position controller. The controller is used in torque control mode so that the motion of the coarse stage can be synchronised with that of the coarse

stage. In this mode, the drive acts as an amplifier, converting a voltage control signal into the required current to drive the actuator.

The *Aerotech ABL10100LT* also has a built in linear encoder with a resolution of 10 nm. It provides a quadrature encoder signal that can be converted to a position measurement.

4.1.2. FINE STAGE

ACTUATION

The fine stage, as discussed earlier, is actuated by a Lorentz actuator. Lorentz actuators are characterised by their linearity and high force predictability, making it an ideal choice for such a high precision application. A Lorentz force is generated between the stator and the mover. Lorentz force is the interaction between a current carrying wire in the shape of a coil and the magnetic field of the permanent magnets. The generated force is linearly proportional to the current through the coil and is given by

$$\mathbf{F} = l_w \cdot \mathbf{I} \times \mathbf{B} \tag{4.1}$$

where $\mathbf{F}$ is the resulting force, l_w is the total length of the current carrying wire in the magnetic field, $\mathbf{I}$ is the current and $\mathbf{B}$ is the magnetic flux density. The specifications of the actuator can be found in Appendix B.1.

AMPLIFIER

The control signal output of the D/A converter of the dSPACE has low voltage and low current. This control signal is amplified in order to be applied on the actuator, using a current feedback amplifier which shows a linear behaviour and is capable of providing bidirectional current. The inductive load of the coil acts as a low pass filter, decreasing current output at higher frequencies. The current feedback applied produces an output current independent of the frequency dependent impedance of the actuator. The decreasing currents at high frequencies are compensated by applying a higher output voltage.

The resistive- inductive load of the actuator creates a resonance between the coil inductance and the internal capacitance of the op-amp, which has been measured to be at 17 kHz. Also, the amplifier was shown to have a flat response upto 1 kHz, after which the phase starts to decrease [16]. More information can be found in Appendix B.2.

SENSOR

The position of the fine stage is measured using a Renishaw RLE10 laser interferometer. It uses a 633 nm Helium - Neon laser source and employs a double pass plane mirror configuration. The output voltage signal is internally converted to a digital quadrature signal, from which the position measurement can be obtained. The resolution of the interferometer is 10 nm.

MECHANICAL DESIGN

The desired 1 DOF motion of the fine stage is achieved using four parallel plate springs, which appropriately constrains the system. The parasitic motion in the vertical direction is a disadvantage in this design. However it is relatively small (0.375 mm) within the ±5 mm horizontal range of the stage. The stiffness in the translational direction of the linear guide, taking into consideration the effect of pre-load caused by the weight of the mover is given by Equation 4.2.

$$k_x = 4 \cdot \frac{12EI}{L^3} - \frac{6F_y}{5L} \tag{4.2}$$

where E is the Young's modulus, I is the moment of inertia, L the length of the plate spring and F_y the pre-load force.

The Lorentz actuator is placed in such a way that the actuation forces act in line with the center of mass, which occurs at the point of symmetry of the parallel plate spring guide. The sensor is placed in such a way that the position measurement is done in line with the actuation forces and the center of mass. This ensures that the influence of possible rotations of the mover have the least effect on the position measurement.

The original system had additional magnets attached to the stator and mover of the fine stage in order such that the magnets act virtually as a nonlinear spring. This is done to obtain a nonlinear force-displacement curve which provides high acceleration and deceleration forces, thereby reducing control input and the resulting Joule heating in the actuator. The drawback is that the nonlinearity must be considered as a disturbance and compensated for. In order to reduce the complexity, these magnets were removed from the fine stage. Stiffness of leaf flexures was increased from 24 N m to 174 N m in order to compensate for the reduction in translational stiffness.

4.2. SYSTEM IDENTIFICATION

4.2.1. DYNAMIC MODEL

A simplified dynamic model of the system must be established to predict the behaviour of the system. The dual stage is modelled to be a double mass-spring-damper system shown in Figure 4.4. The behaviour of the system is described by the following two equations in the Laplace domain.

$$m_{cs}s^2 + (c_{cs} + c_{fs})s + (k_{cs} + k_{fs}))X_{cs}(s) - (c_{fs}s + k_{fs})X_{fs}(s) = F_{cs}(s) - F_{fs}(s) \tag{4.3a}$$

$$(m_{fs}s^2 + c_{fs}s + k_{fs})X_{fs}(s) - (c_{fs}s + k_{fs})X_{cs}(s) = F_{fs}(s) \tag{4.3b}$$

From (4.3a) and (4.3b) the four transfer functions from the input forces F_{cs} and F_{fs} to the stage positions x_{cs} and x_{fs} can be derived, which describe the response of the system.

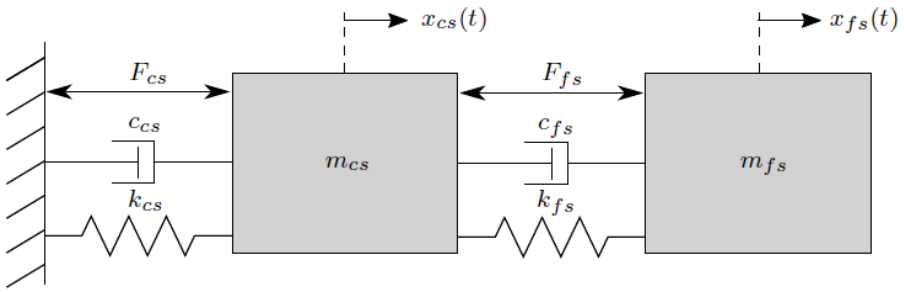

Figure 4.4: Dual positioning stage modeled as mass spring damper system. Image courtesy [16]

$$G_{cs,cs}(s) = \frac{x_{cs}}{F_{cs}} \qquad G_{cs,fs}(s) = \frac{x_{cs}}{F_{fs}}$$
$$G_{fs,cs}(s) = \frac{x_{fs}}{F_{cs}} \qquad G_{fs,fs}(s) = \frac{x_{fs}}{F_{fs}} \tag{4.4}$$

Here $G_{cs,cs}$ and $G_{fs,fs}$ are the transfer functions that need to be considered while designing the controllers. $G_{cs,cs}$ describes how the coarse stage position reacts to a force input of the coarse stage actuator and $G_{fs,fs}$ describes how the fine stage position reacts to a force input of the fine stage actuator. The off-diagonal terms $G_{cs,fs}$ and $G_{fs,cs}$ are referred to as the cross-coupling terms, essentially describing the mechanical coupling between the two stages.

The transfer functions are

$$G_{cs,cs}(s) = \frac{m_{fs}s^2 + c_{fs}s + k_{fs}}{(m_{fs}s^2 + c_{fs}s + k_{fs})(m_{cs}s^2 + (c_{fs} + c_{cs})s + k_{fs} + k_{cs}) - (c_{fs}s + k_{fs})^2} \tag{4.5}$$

$$G_{cs,fs}(s) = \frac{-m_{fs}s^2}{(m_{fs}s^2 + c_{fs}s + k_{fs})(m_{cs}s^2 + (c_{fs} + c_{cs})s + k_{fs} + k_{cs}) - (c_{fs}s + k_{fs})^2} \tag{4.6}$$

$$G_{fs,cs}(s) = \frac{c_{fs}s + k_{fs}}{(m_{fs}s^2 + c_{fs}s + k_{fs})(m_{cs}s^2 + (c_{fs} + c_{cs})s + k_{fs} + k_{cs}) - (c_{fs}s + k_{fs})^2} \tag{4.7}$$

$$G_{fs,fs}(s) = \frac{m_{cs}s^2 + c_{cs}s + k_{cs}}{(m_{fs}s^2 + c_{fs}s + k_{fs})(m_{cs}s^2 + (c_{fs} + c_{cs})s + k_{fs} + k_{cs}) - (c_{fs}s + k_{fs})^2} \tag{4.8}$$

4.2.2. FREQUENCY RESPONSE ESTIMATION

In order to model the dynamics of the plant described in section 4.2.1, known input signals are applied to the system and the frequency response is measured. White noise and frequency sweep of 0.1 to 2000 Hz are used as input signals. Sufficient amplitude of force inputs were chosen to give a small but a detectable response. With known force input and

position output data, frequency response function can be calculated as

$$H(f) = \frac{\sum_{i=1}^{N} Y_i(f) U_i^*}{\sum_{i=1}^{N} U_i(f) U_i^*} \tag{4.9}$$

where U_i^* and Y_i^* are the input and output fourier transforms respectively. This calculation was performed using the function `etfe` in MATLAB. The obtained frequency response and identified system can be found in Figure 4.5. Resonance frequencies of the system are around 2.5 Hz and 4.5 Hz.

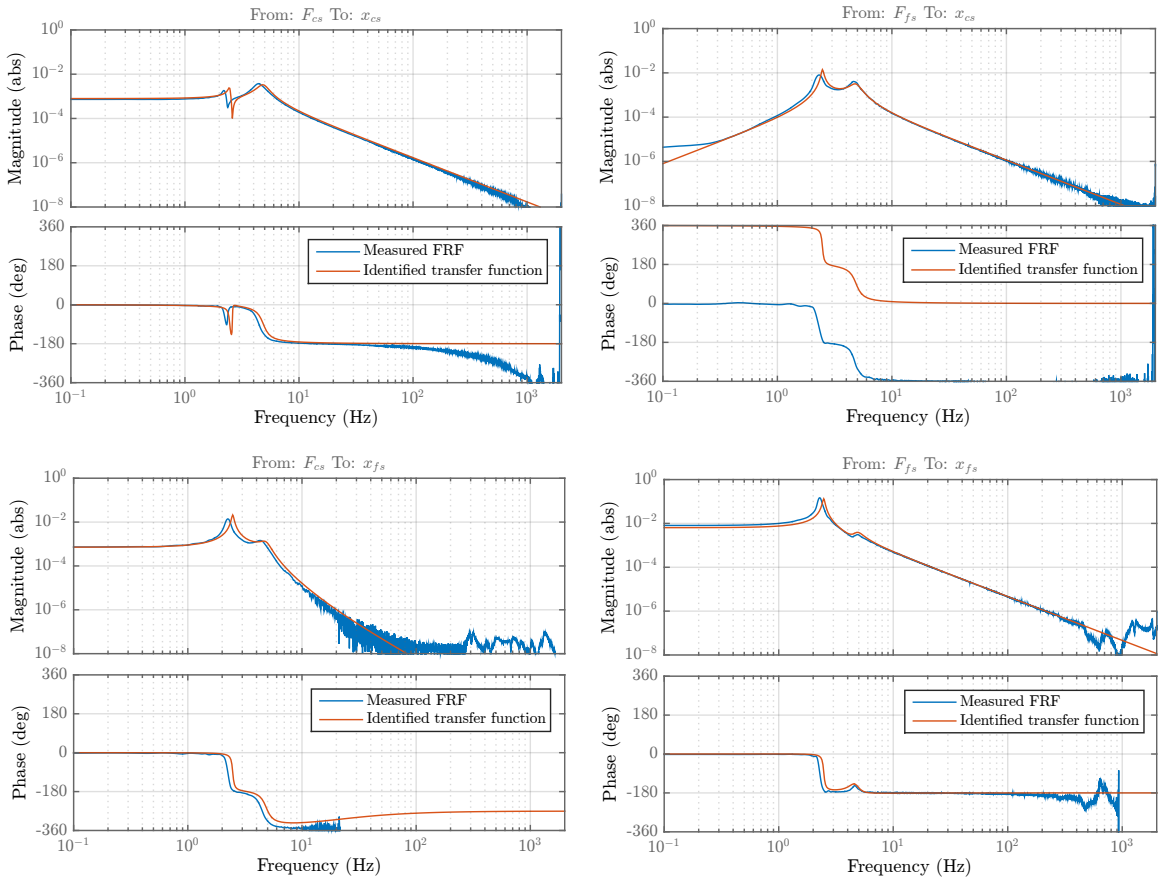

Figure 4.5: Measured frequency response function and identified transfer functions of the system.

From the coarse stage response $G_{cs,cs}$ it can be seen that the measured response shows an additional phase lag starting at around 40 Hz. This additional phase lag is caused by the phase delay of the amplifier. In the response of the fine stage, a higher order resonance can be observed at approximately 1000 Hz. Also, a small additional phase lag is observed starting at around 100 Hz. In the estimated response, these behaviour are not captured.

These additional phase lags and dynamics would act as a limiting factor in achieving high control bandwidths and must be taken into account in designing the controllers. Also, this makes the chosen plant an ideal system to test the developed control techniques.

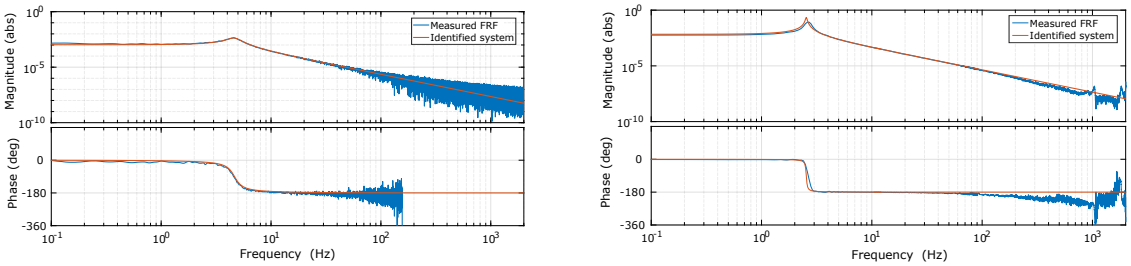

(a) (b)

Figure 4.6: Measured and estimated responses of (a) coarse stage (b) fine stage

4.2.3. IDENTIFICATION IN TIME DOMAIN

In order to determine the parameters of the plant, system identification was done in the time domain, by trying to minimise the error between the simulated output and the measured output. This was modelled as an optimisation problem in MATLAB, with the objective function being the error.

To obtain appropriate initial values that are close to the ideal parameters, the coarse stage and the fine stage were mounted separately to the optical test unit. The frequency response functions of the two stages can be modelled as two mass -spring -damper systems with second order transfer functions. The transfer functions G_{cs} and G_{fs} for the coarse and fine stages respectively are given below:

$$G_{cs} = \frac{1}{m_{cs}s^2 + c_{cs}s + k_{cs}} \tag{4.10}$$

$$G_{cs} = \frac{1}{m_{fs}s^2 + c_{fs}s + k_{fs}} \tag{4.11}$$

The function `lsqnonlin` of the optimisation toolbox in MATLAB was used for the nonlinear optimisation problem. For the identification of the coarse stage, a white noise input signal is used, and another dataset for a white noise sequence is used for validation. Parameter optimisation for the fine stage was done using a filtered chirp signal and then validated using a white noise signal. For each case, the VAF was also calculated to ensure the validity of the results and were found to be higher than 99% for all cases. The measured and simulated responses can be found in Figure 4.7 and Figure 4.8 for the coarse and fine stages respectively.

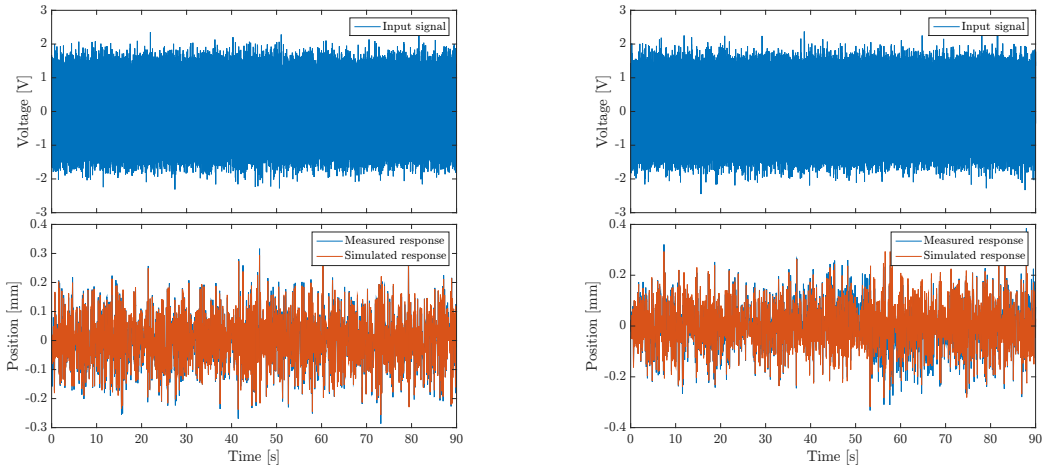

(a) Identification dataset (b) Validation dataset

Figure 4.7: Simulated response versus measured response of the coarse stage

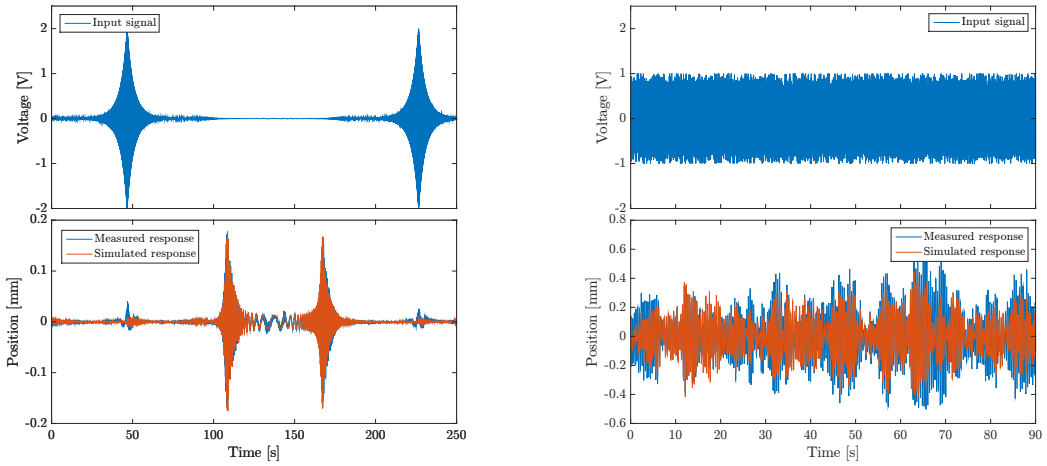

(a) Identification dataset (b) Validation dataset

Figure 4.8: Simulated response versus measured response of the fine stage

The identified frequency responses of the two stages together with their modelled responses are shown in 4.6a and 4.6b.In this figure, the parameters are updated to match the modeled responses to the measured responses. The identified transfer functions would also be useful in conducting tests on the stages separately.

Attempts to identify the overall system using the identified parameters using an optimization algorithm were not successful as the algorithm did not converge.

4.2.4. FREQUENCY DOMAIN IDENTIFICATION

The identification of the MIMO system was hence carried out as a grey box identification problem. The MATLAB function `tfest` was used to fit the transfer function $G_{cs,cs}(s)$. Once

this was done, the same denominator is applicable for other transfer functions of the MIMO system, and only the zeros had to be ascertained. This was done using the parameters identified earlier. The transfer function gains were manually adjusted.

Validation of the ascertained parameters was done by simulating the response to a filtered chirp signal and a white noise input. The simulated responses were checked to closely resemble the measured responses, as can be seen in Figure 4.9. VAF was calculated to be 97.6% and 97.2% for the two responses respectively. The final parameters used in the model are given in Table 4.1.

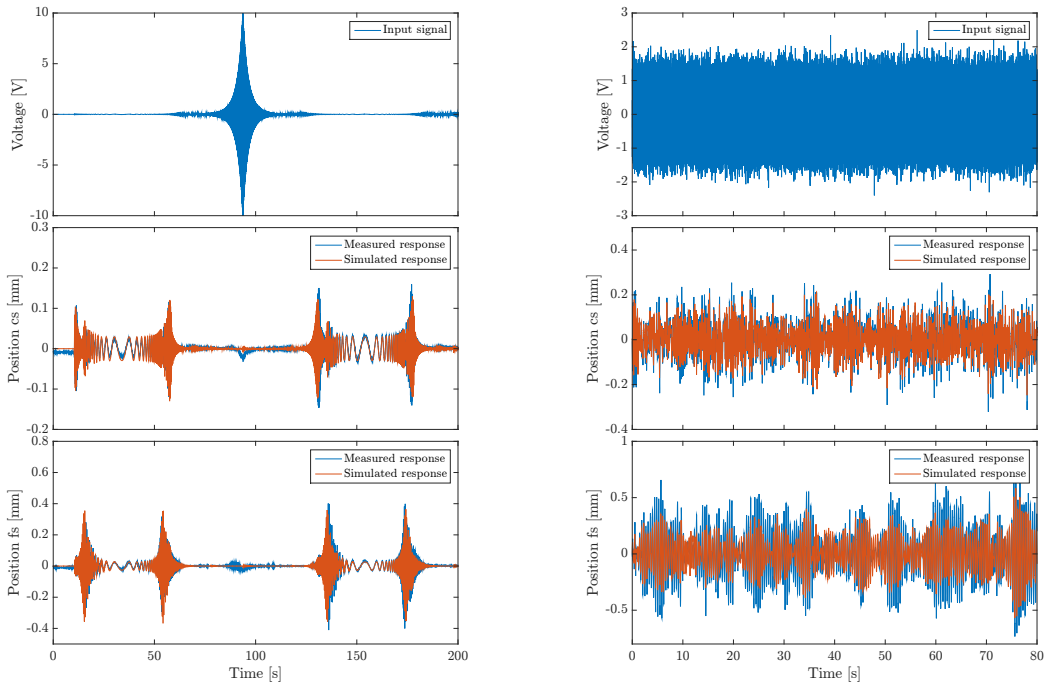

(a) Chirp signal

(b) Noise signal

Figure 4.9: Validation of the identified system

Parameter	Value	Unit
m_{cs}	2.34	kg
c_{cs}	17	$\mathrm{N\,s\,m^{-1}}$
k_{cs}	2000	$\mathrm{N\,m^{-1}}$
m_{fs}	0.57	kg
c_{fs}	0.28	$\mathrm{N\,s\,m^{-1}}$
k_{fs}	146	$\mathrm{N\,m^{-1}}$

Table 4.1: Model Parameters

4.3. BANDWIDTH REQUIREMENTS FOR PRECISION

The system must have a certain minimum stiffness to achieve the desired levels of accuracy, as the stiffness determines the natural frequency of the system. It is known that this natural frequency is directly related to the performance of the system with respect to rejecting external vibration disturbances [2]. It has also been shown in [2] that a virtual stiffness can be created between the metrology frame and the moving mass using a feedback controller. However, to sufficiently reject the disturbances, the controller should have a certain minumum bandwidth. This minimal bandwidth is calculated in this section.

4.3.1. COARSE STAGE

The main source of disturbance acting on the coarse stage is assumed to be disturbances forces caused by reset of the fine stage controller. An accelerometer was employed to measure these accelerations. For a step of 0.1 µm, the accelerations were measure to be 1.2 m/s^2. Assuming that the coarse stage has a low stiffness and damping, the required control forces to counteract the disturbances are equal to

$$F_{control} = ma_{vib} \tag{4.12}$$

where m is the moving mass of the coarse stage and a_{vib} the maximum acceleration of the vibrations. When a simple controller with only a proportional gain k_p is used, the control forces of the controller are given by

$$F_{control} = k_p \epsilon_{max,cs} \tag{4.13}$$

where $\epsilon_{max,cs}$ is the maximum allowed tracking error of the coarse stage. The controller bandwidth f_{bw} in Hz can then be calculated using

$$f_{bw} = \frac{1}{2\pi}\sqrt{\frac{k_p}{m}}. \tag{4.14}$$

Combining Equations (4.12) - (4.14) yields :

$$f_{bw} = \frac{1}{2\pi}\sqrt{\frac{a_{vib}}{\epsilon}}. \tag{4.15}$$

With the maximum tracking error for the coarse stage limited to 10 µm and disturbances in the form of accelerations of 1.2 m/s^2, a bandwidth of atleast 54 Hz is required.

4.3.2. FINE STAGE

The main forces acting on the fine stage arise out of the tracking error of the coarse stage and the transmission of external vibrations to the fine stage. In the optical test facility on

which the system is mounted, Vibration Criterion A (VC-A) is assumed to be valid. The RMS velocity is given to be $50\,\mu m\,s^{-1}$ from which the maximum velocity v_{max} can be calculated. The total control force required to compensate for the disturbances is thus given by

$$F_{control} = c_{fs} v_{max} + \epsilon_{max,cs} k_{fs}. \tag{4.16}$$

Taking a maximum allowable position error of 10 nm , and using Equations (4.12) - (4.14), we calculate the required control bandwidth for the fine stage as

$$f_{bw} = \frac{1}{2\pi}\sqrt{\frac{c_{fs} v_{max} + \epsilon_{max,cs} k_{fs}}{\epsilon_{max,fs} m_{fs}}} = 81.1\,\text{Hz} \tag{4.17}$$

Also, the minimum stiffness for achieving a precision of 10 nm can be calculated as

$$k_{fs,min} = \frac{c_{fs} v_{max} + \epsilon_{max,cs} k_{fs}.}{\epsilon_{max,fs}} = 1.48 \times 10^5\,\text{N m}^{-1} \tag{4.18}$$

Assuming a saturation voltage of 3 V($1A$), the active stiffness was found to be $1.65 \times 10^8\,\text{N m}^{-1}$. This validates the design choice of fixing the fine stage stiffness at $146\,\text{N m}^{-1}$, as the active stiffness has been shown to be higher than the stiffness needed to achieve the desired precision.

5

CONTROLLER DESIGN

In this chapter, the control structure used for reset controllers is introduced. Implementation of the controllers in discrete time state space form within the MATLAB/Simulink environment is then discussed. Following this, the three reset controllers developed in chapter 3 are tuned for the fine stage of the experimental setup discussed in chapter 4. A linear PID controller is also tuned based on guidelines given in subsection 1.1.2. Open loop frequency response is estimated through describing functions for the reset controllers and compared with PID.

5.1. RESET CONTROL STRUCTURE

Reset elements, by definition operate on the error signal, with reset occurring at the zero crossings of error. Thus the reset element must be the first element in the control loop. The reset part is placed first in the control loop and the non reset part is placed in series. A block diagram depicting the structure of reset PID controllers is shown in Figure 5.1. The state space representations are as follows :

$$\Sigma_r := \begin{cases} \dot{x}_r(t) = A_r x_r(t) + B_r e(t), & e(t) \neq 0 \\ x_r(t^+) = A_\rho x_r(t), & e(t) = 0 \\ u_r(t) = C_r x_r(t) + D_r e(t) \end{cases} \tag{5.1}$$

$$\Sigma_{nr} := \begin{cases} \dot{x}_{nr}(t) = A_{nr} x_{nr}(t) + B_{nr} u_r(t), \\ u_{nr}(t) = C_{nr} x_{nr}(t) + D_{nr} u_r(t) \end{cases} \tag{5.2}$$

$$\Sigma_{RC} := \begin{cases} \dot{x}_{RC}(t) = A_{RC} x_{RC}(t) + B_{RC} e(t), & e(t) \neq 0 \\ x_{RC}(t^+) = \bar{A}_\rho x_{RC}(t) & e(t) = 0 \\ u(t) = C_{RC} x_{RC}(t) + D_{RC} e(t) \end{cases} \tag{5.3}$$

where $e(t)$ is the error signal, $u_r(t)$ is the output of the reset part, which is given as input to the nonlinear component. $u(t)$ is the control input to the plant. The reset controller states, nonlinear controller states, and reset PID states are given by $x_r(t), x_{nr}(t)$ and $x_{RC}(t) = [x_r^T \; x_{nr}^T]^T$ respectively. The reset matrices for the reset component and for the reset

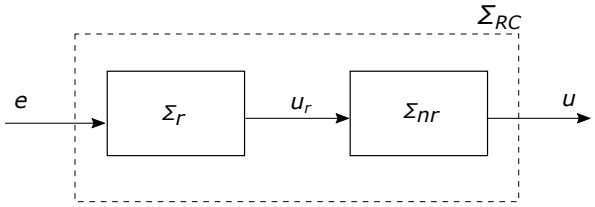

Figure 5.1: The reset PID controller is split into two components, the reset part and the non reset part.

PID are given by A_ρ and $\bar{A}_\rho$ respectively. A_{RC}, B_{RC}, C_{RC}, and D_{RC} are state space matrices of the base linear controller and are given by

$$\begin{aligned} A_{RC} &= \begin{bmatrix} A_r & 0 \\ B_{nr}C_r & A_{nr} \end{bmatrix}, \\ B_{RC} &= \begin{bmatrix} B_r \\ B_{nr}D_r \end{bmatrix} \\ C_{RC} &= \begin{bmatrix} D_{nr}C_r & C_{nr} \end{bmatrix}; \\ D_{RC} &= D_{nr}D_r \end{aligned} \tag{5.4}$$

where reset matrix $\bar{A}_\rho$ is given by

$$\bar{A}_\rho = \begin{bmatrix} A_\rho & 0 \\ 0 & I_{n_{nr}} \end{bmatrix} \tag{5.5}$$

where n_{nr} is the number of non reset control states.

5.2. CONTROLLER IMPLEMENTATION

The reset controllers are implemented in the system in discrete time. The controllers tuned in continuous time are discretized using the MATLAB function *c2d*. A sampling frequency of 20 kHz was chosen, which is much higher than the sampling frequency mandated for the control bandwidths to be used. This was the maximum frequency that can be applied in the dSPACE interface. The discrete time state space is given by

$$\Sigma_{RC} := \begin{cases} x[k+1] = A_d x[k] + B_d e[k], & e[k] \neq 0 \\ x[k+1] = A_\rho x[k], & e[k] = 0 \\ u[k] = C_d x[k] + D_d e[k] \end{cases} \tag{5.6}$$

where A_d, B_d, C_d, D_d are the discrete time state space matrices corresponding to A_{RC}, B_{RC}, C_{RC}, and D_{RC}. The state space representation was implemented in Simulink as shown in Figure 5.2.

Parameter	Controller A	Controller B	Controller C
ω_c	150	200	150
K_p	9.24×10^5	1.74×10^6	3.09×10^5
ω_i	$\omega_c/10$	$\omega_c/10$	$\omega_c/10$
ω_d	$\omega_c/5$	$\omega_c/5$	$\omega_c/3$
ω_τ	-	-	$\omega_c \times 3$
α	0.7	0.7	-
ω_l	$\omega_c \times 7$	$\omega_c \times 7$	$\omega_c \times 4.5$

Table 5.1: Controller Parameters

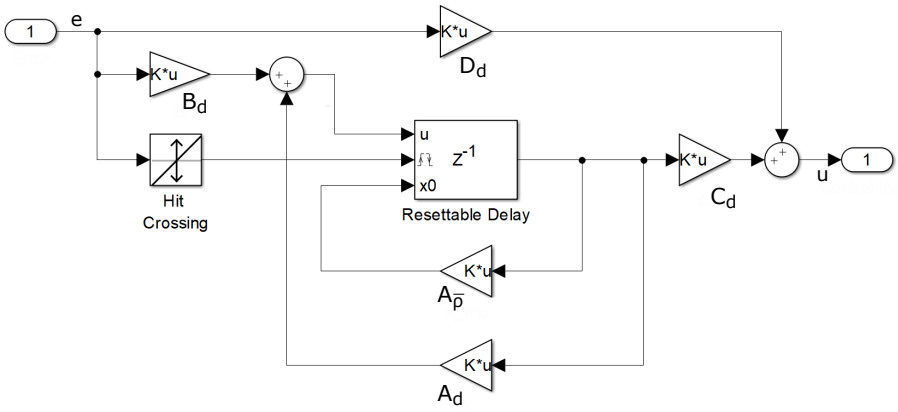

Figure 5.2: Block diagram for Reset PID in discrete time

5.3. CONTROLLER PARAMETERS

All developed controllers were tuned for the fine stage in the experimental setup, to have a phase margin of 45°. Also, a PID controller is tuned so that the improvement in performance using reset PID can be validated. Bandwidth for the PID controller is chosen as 150 Hz, which is higher than the minimum bandwidth calculated in section 4.3. The cutoff frequencies for the integrator, differentiator and the taming pole are chosen as per the rules of thumb. A first order low pass filter is placed at a frequency of 900 Hz, which is 6 times higher than the bandwidth. The targets for bandwidth and phase margin were met with these parameters.

Parameters in (3.3) and (3.4) for the three reset controllers are tabulated in Table 5.1. Open loop for all controllers are estimated using describing functions and are compared with PID in Figure 5.3.

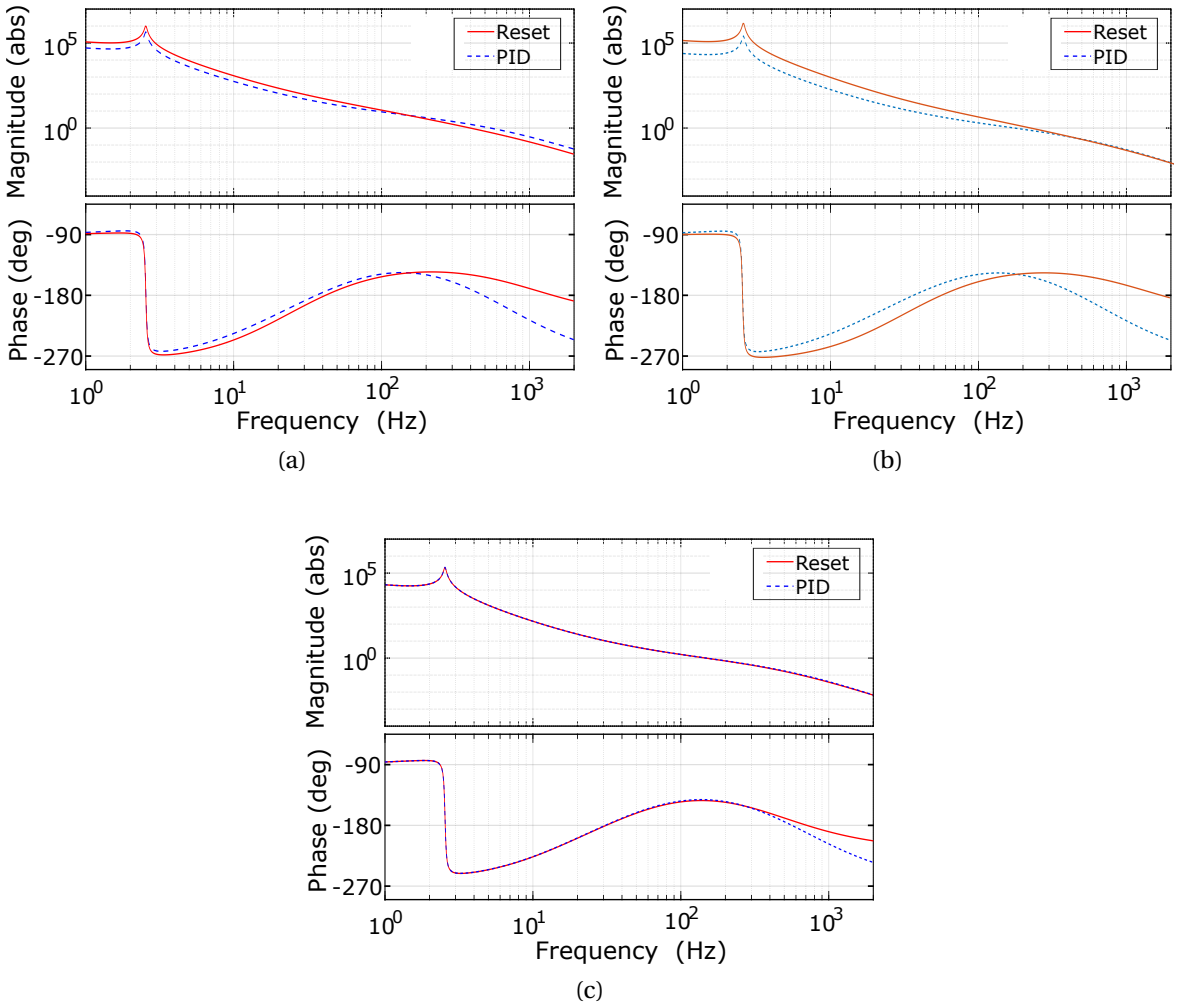

Figure 5.3: (a) Case 1 - comparison of open loop for Reset controller A vs PID. (b) Case 2 - comparison of open loop for Reset controller B vs PID. (c) Case 3 - comparison of open loop for Reset controller C vs PID.

6

EXPERIMENTAL VERIFICATION

The controllers that were tuned in section 5.3 are implemented in the setup and experiments are conducted to validate the controllers performance. The fine stage has been removed from the coarse stage for this set of experiments because the plant is now a second order system and the effect of change in controller parameters will be more readily perceivable. The practical experiments conducted in both time domain and frequency domain are explained and the results are shown. In the time domain, reference tracking performance and steady state precision in the presence of noise are analyzed. In frequency domain, sensitivity function and complementary sensitivity function are computed and compared with the estimations made from describing functions.

6.1. TIME DOMAIN

6.1.1. REFERENCE TRACKING

A fourth order motion profile, as developed in [17] was applied to the stage to study the reference tracking performance. By imposing limits on the first four derivatives of position (velocity, acceleration, jerk, and snap), a prefiltered trajectory was created, the demands of which are much lesser than the physical limits of the system. Such a profile also limits the high frequency content in the reference signal, reducing the demands on the feedback controller. Also, in [17], a feedforward was proposed to improve the tracking performance, which essentially is an inverse of the plant transfer function. The DC gain of the feedforward equals the inverse DC gain of the plant, which has been shown in [18] to be necessary for better set point regulation and to avoid limit cycles.

The parameters used to generate the trajectory are listed in Table 6.1

Controller	Maximum Steady State Error (nm)	RMS Tracking Error (nm)
PID	40	41.48
Controller A	20	23.12
Controller B	40	15.73
Controller C	30	43.15

Table 6.2: Comparison of maximum steady state errors and RMS tracking errors for the developed controllers.

Parameter	Value
Displacement	400 µm
Maximum velocity	$7.5\,\mathrm{mm\,s^{-1}}$
Maximum acceleration	$5\,\mathrm{cm/s^2}$
Maximum jerk	$1\,\mathrm{m/s^3}$
Maximum snap	$10\,\mathrm{m/s^4}$

Table 6.1: Amplitude and the constraints on the derivatives of the fourth order profile

The control structure used is shown in Figure 6.1. The gains q1, q2, q3, q4, and the parameters of the discrete filter are calculated as given in [17].

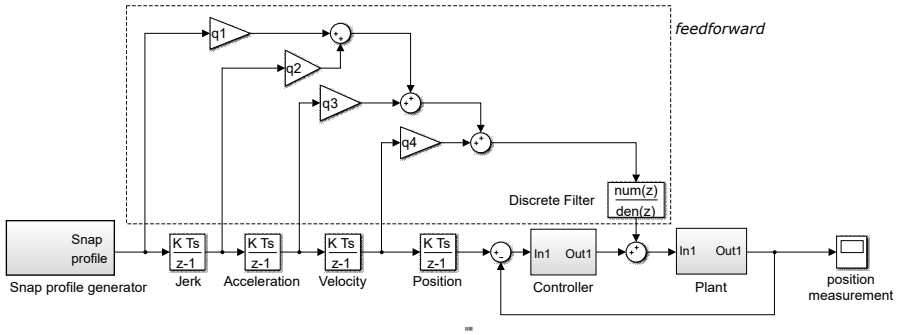

Figure 6.1: Control structure used for reference tracking

The tracking errors obtained with the 3 reset controllers are compared with the tracking error from PID in Figure 6.2. The RMS values of tracking errors are tabulated in Table 6.2. The RMS error for Controller A has reduced by 34 % compared to PID. This can be explained by the higher low frequency gain of Controller A. The reduction for Controller B is even higher, at around 60 %. This also is as expected, since by increasing bandwidth, the gain of Controller B at lower frequencies is greater than that of controller A. This reduction is the highest among the 3 controllers. Reset controller C does not show any improvement in the tracking performance.

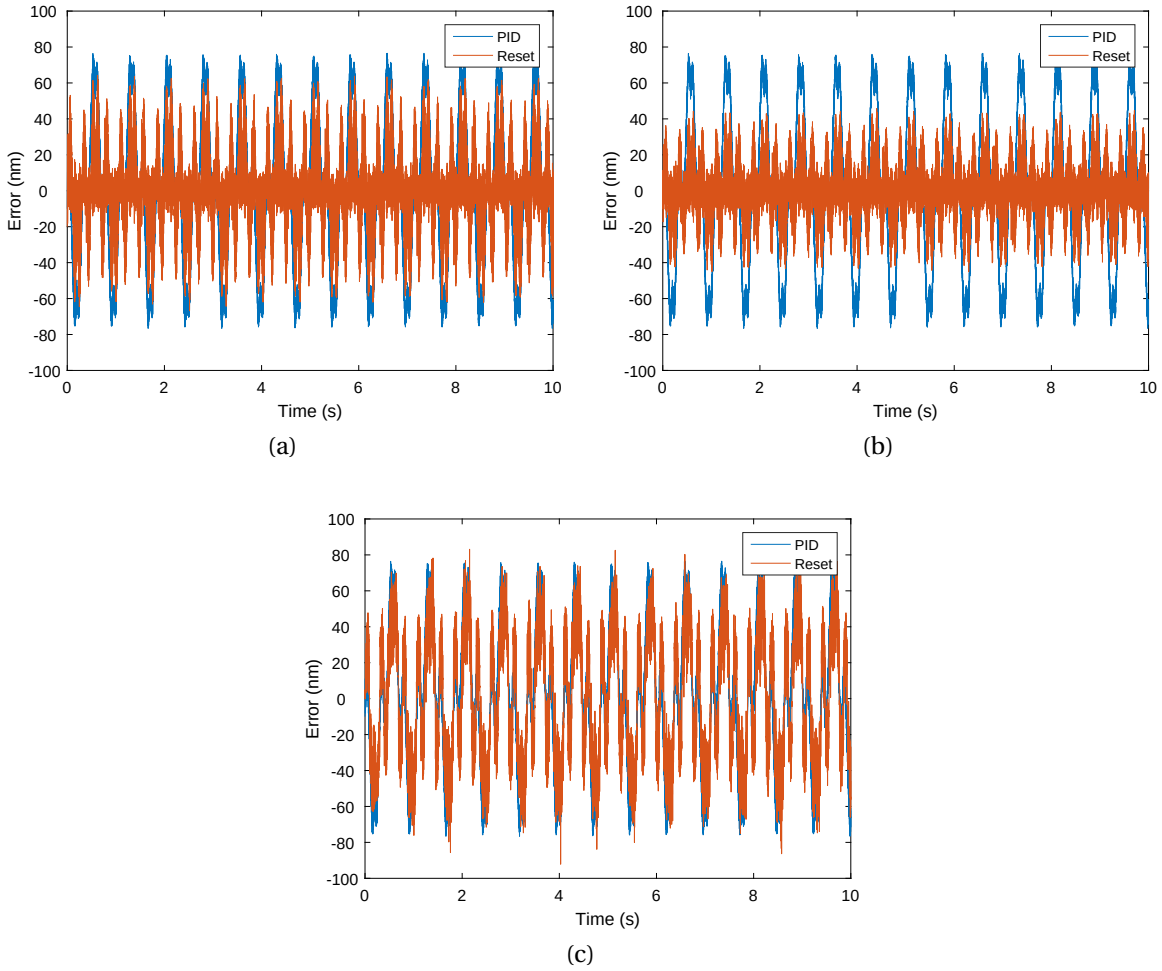

Figure 6.2: (a) Case 1 -Tracking error for Reset controller A vs PID. (b) Case 2 - Tracking error for Reset controller B vs PID. (c) Case 3 - Tracking error for Reset controller C vs PID.

6.1.2. STEADY STATE PRECISION

The steady state performance of the controllers was studied to validate the improvement in precision predicted in the describing function analysis. In steady state, with only the sensor noise present in the system, the achieved precision was 10 nm for all the three controllers, which is equal to the resolution of the interferometer used. So, white noise of amplitude 50 nm was added as measurement noise n as shown in Figure 6.3 and the error signal was measured.

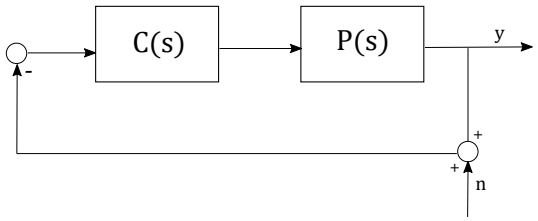

Figure 6.3: Block diagram showing additional noise added for closed loop identification

The measured error signals obtained with the three reset controller cases are compared

with the error obtained from PID in Figure 6.4. The maximum values of errors are tabulated in Table 6.2.

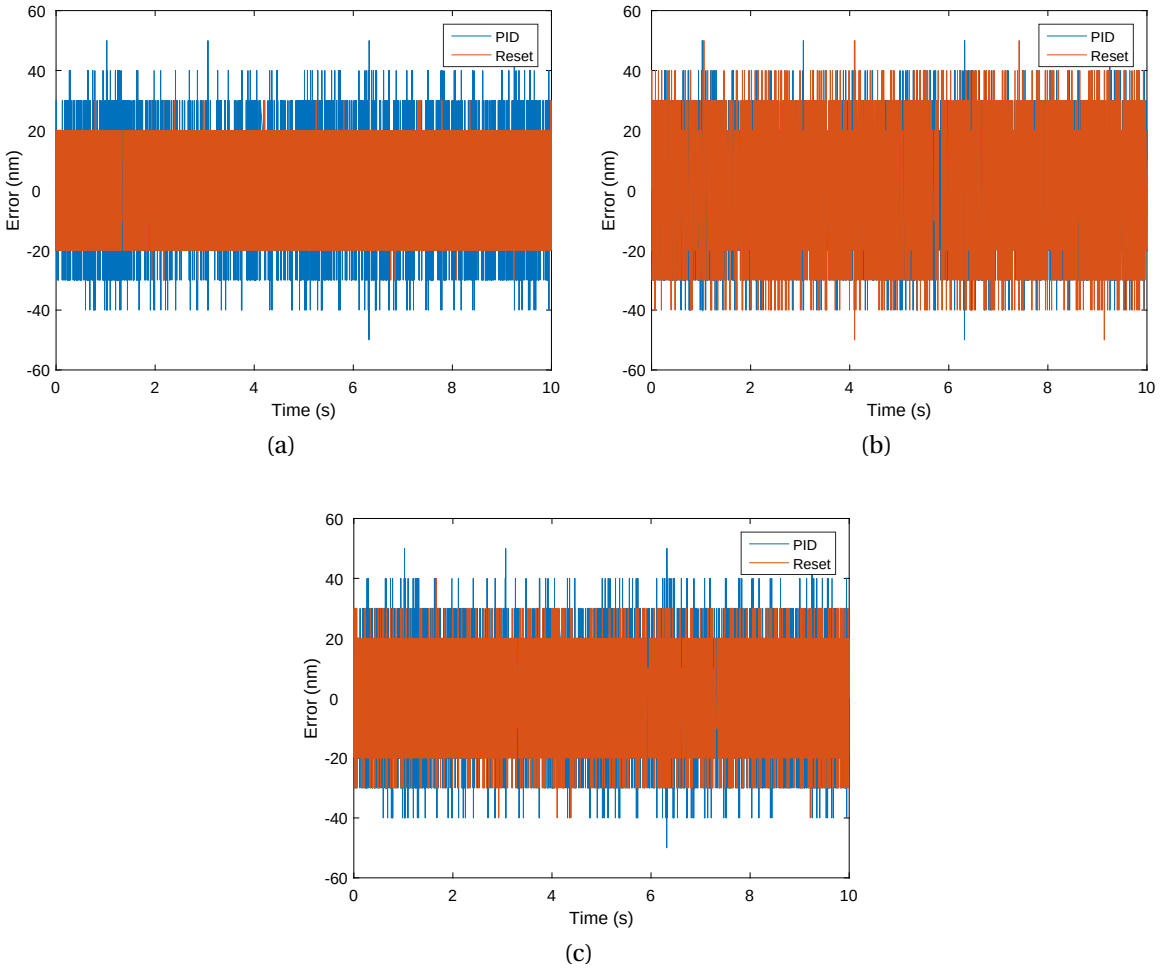

Figure 6.4: (a) Case 1 - steady state error for Reset controller A vs PID. (b) Case 2 - steady state error for Reset controller B vs PID. (c) Case 3 - steady state error for Reset controller C vs PID

The maximum steady state error has been shown to have improved from 40 nm for the PID to 20 nm for controller A, and 30 nm for controller C. The bandwidth of Controller B was gradually increased from 150 Hz. It was observed that the steady state error increased with increase in bandwidth and at a bandwidth of around 200 Hz, it became equal to that of the PID. Thus, a bandwidth improvement of 33 % has been achieved.

6.2. FREQUENCY DOMAIN

The sensitivity function and the complementary sensitivity function were identified by adding chirp noise as measurement noise in the closed loop system depicted in Figure 6.3. The signal is a bidirectional logarithmic frequency sweep from 0.1 Hz to 2000 Hz for a time duration of 8 minutes, with a target time of 120 seconds. An amplitude of 1 µm was chosen, and the signal was filtered with a low pass filter to sufficiently attenuate the higher frequencies and thereby limit the control input to within saturation levels.

Having measured the noise input and the position output, the sensitivity function and the complementary sensitivity function were identified using the MATLAB function *etfe*. Sensitivity function was obtained as the transfer from n to $y+n$, and the complementary sensitivity function as the transfer from $-n$ to y.

The identified sensitivity functions for the three controllers compared with sensitivity functions estimated from describing function analysis in Figure 6.6. Similarly, the complementary sensitivity functions are compared in Fig. Figure 6.5. It can be seen that the measured responses match well with the estimated responses. From Fig. 6.5b, it can be seen that the bandwidth has been increased from 150 Hz to around 200 Hz by Controller B, which is an improvement of 33 %. Though the bandwidths achieved are as expected, the sensitivity peaks in the identified responses for controllers A and B are slightly higher than with describing functions, which shows that reset has added marginally lesser phase than anticipated from describing functions, which can be attributed to the phase delay introduced by discretization. This is not the case with controller C, as reset was not used in this case to add phase at bandwidth. The better tracking performance of controller B can be explained by the lower sensitivity shown by controller B at low frequencies compared to controller A in 6.6a and 6.6b. In 6.5c, a reduction in complementary sensitivity can be seen at high frequencies, which indicates improvement in precision. Apart from the deviations between the expected and measured frequency responses described above, describing functions provide a good approximation of reset behavior in the three controllers.

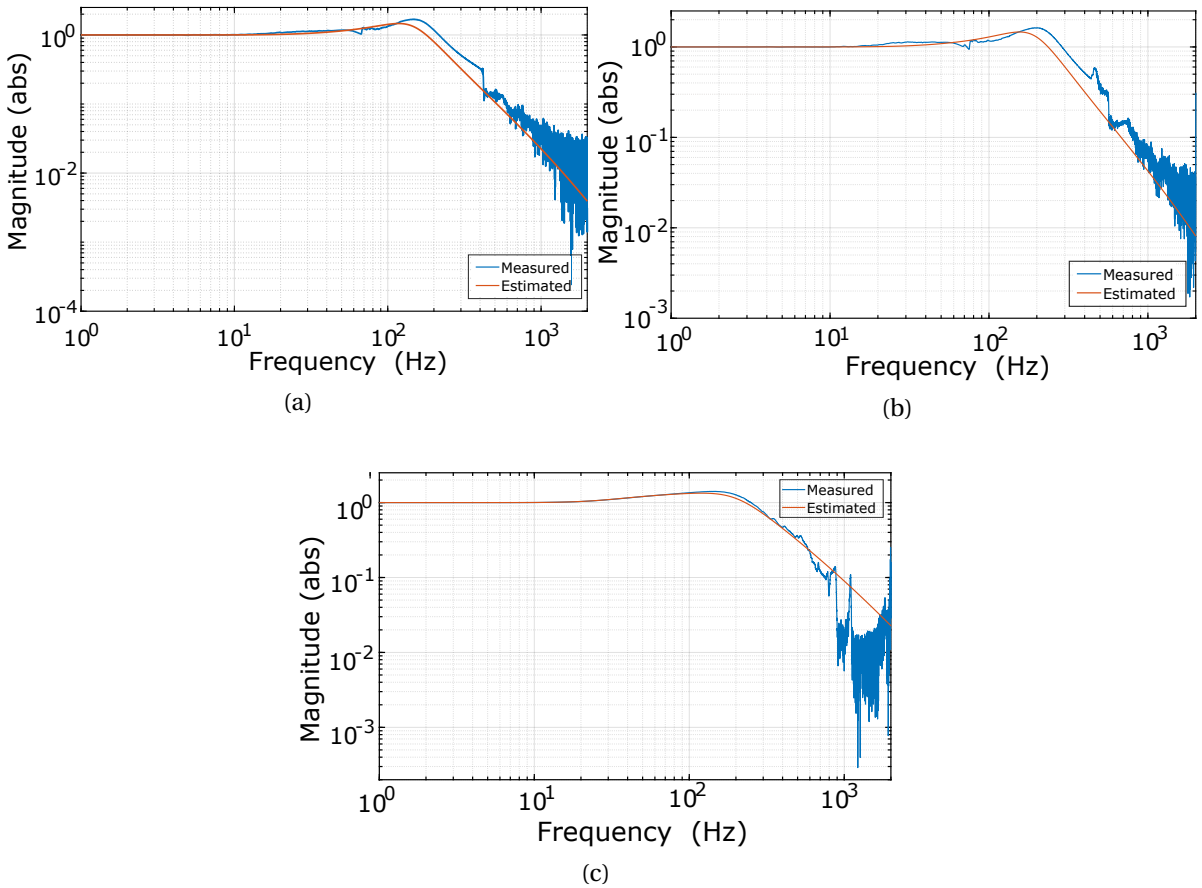

Figure 6.5: (a) Case 1 - Measured vs Estimated complementary sensitivity function for Reset controller A. (b) Case 2 - Measured vs Estimated complementary sensitivity function for Reset controller B. (c) Case 3 - Measured vs Estimated complementary sensitivity function for Reset controller C

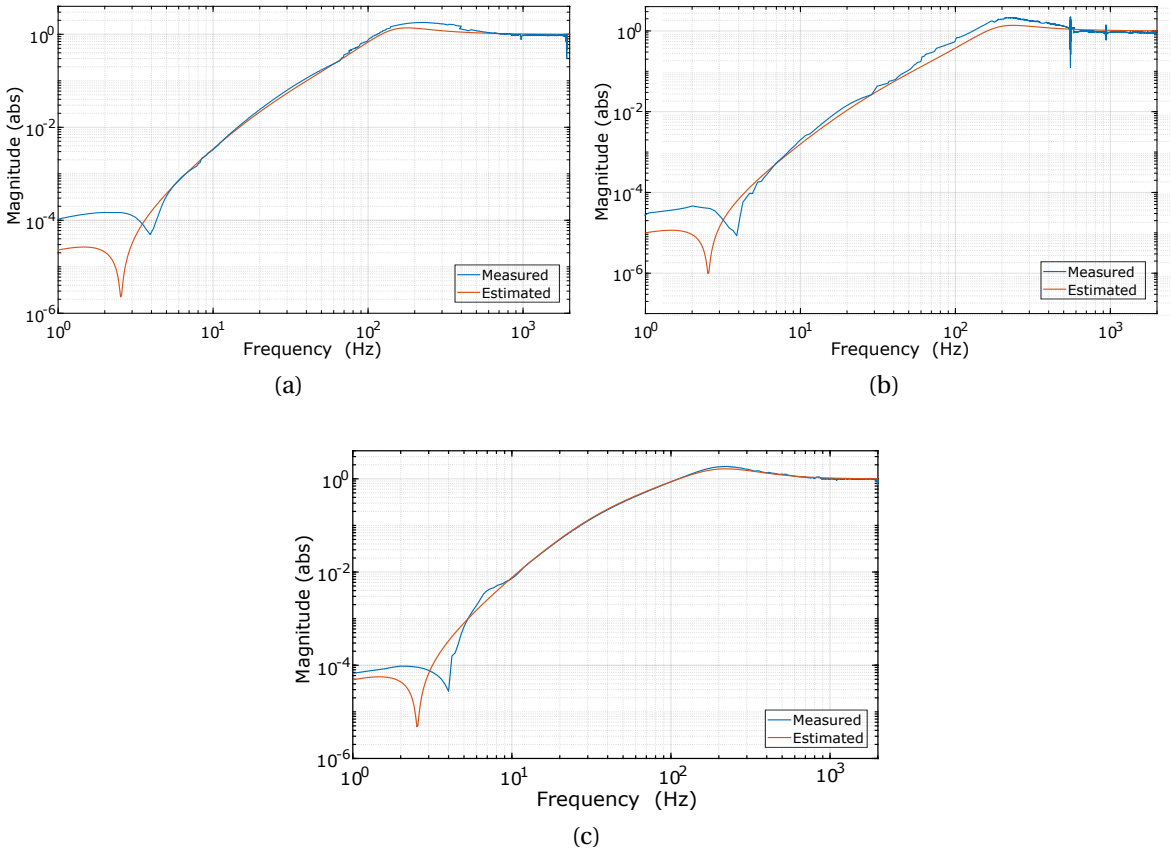

Figure 6.6: (a) Case 1 - Measured vs Estimated sensitivity function for Reset controller A. (b) Case 2 - Measured vs Estimated sensitivity function for Reset controller B. (c) Case 3 - Measured vs Estimated sensitivity function for Reset controller C

7

EXPERIMENTAL RESULTS - DUAL STAGE

In this chapter, performance of reset is investigated in the dual stage setup. The master/slave architecture used to control the two stages is discussed. The concept of decoupling used to reduce the cross-coupling between the two stages is discussed. Following this, the results from reference tracking experiments are discussed.

7.1. CONTROL STRUCTURE

7.1.1. MASTER/SLAVE CONTROL

A master/slave control strategy is a simple but effective way to drive a dual stage positioning system. In this technique, two independent Single-Input-Single-Output (SISO) controllers are used to control the Multiple-Input-Multiple-Output dual stage system. A basic master/slave control scheme that is used is shown in Figure 7.1. In a dual stage positioning system, the fine stage $G_1(s)$ acts as the master. To track the predefined set point, the fine stage position is controlled with a high bandwidth feedback controller $C_1(s)$. The coarse stage $G_2(s)$ is made to act as the slave, that tries to follow the fine stage position as well as possible. This is done by making the position error between the fine stage and the coarse stage as the error signal for the coarse stage controller $G_2(s)$, and as a result the coarse stage position x_2 goes to such a value that the position error becomes zero.

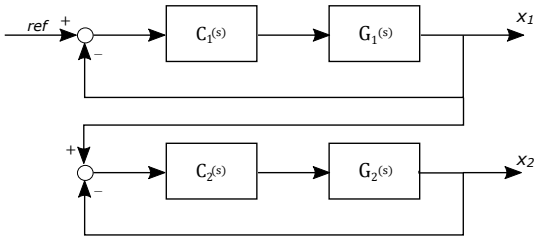

Figure 7.1: The master/slave control scheme used for the dualstage positioning system. $C_1(s)$ and $G_1(s)$ represent the fine stage controller and plant respectively, whereas $C_2(s)$ and $G_2(s)$ denote the coarse stage controller and plant.

7.1.2. DECOUPLING

In the dual stage positioning system, it is inevitable that the control loops affect each other by acting as disturbances. However, since the dynamics of the system are known, they can be considered to be known disturbances. By judicious use of feedforward, these disturbances can be compensated for by a process termed decoupling. It is essentially an attempt to isolate the fine and course stage from each others dynamics.

Decoupling feedforward was applied in the system as given in [19]. The block diagram for this decoupling method is shown in Figure 7.2. Let the transfer functions for *i-th* input $U_i(s)$ to *j-th* output $Y_j(s)$ be defined as $G_{ji}(s)$.

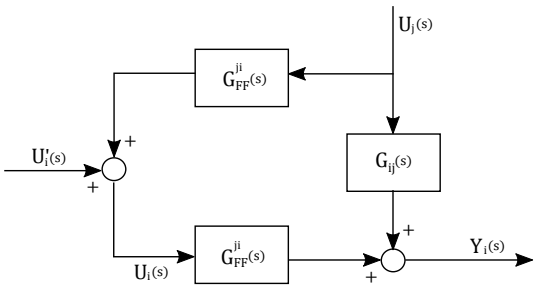

Figure 7.2: Block diagram showing decoupling feedforward

Because of coupling, *j-th* input $U_i(s)$ also has a contribution to output $Y_i(s)$ as follows:

$$Y_i s = G_{ii}(s) + U_i s + G_{ij}(s)U_j(s) \tag{7.1}$$

In order to compensate for the coupling from *j-th* loop to the *i-th* loop in the frequency band $[0\ \omega_{ff}]$, the feedforward gain $G_{FF}^{ji}(s)$ should be chosen such that

$$G_{FF}^{ji}(s)G_{ii}(s) + G_{ij}(s) \approx 0,\ \forall\omega \in [0\ \omega_{ff}] \tag{7.2}$$

This could also be written as,

$$G_{FF}^{ji}(s) = -G_{ii}^{-1}(s)G_{ij}(s) \tag{7.3}$$

7.2. REFERENCE TRACKING

The control structure for reference tracking was constructed based on the master/slave control scheme with decoupling feedforward force, as shown in Figure 7.3. This is in addition to the fine stage feedforward computed from the reference.

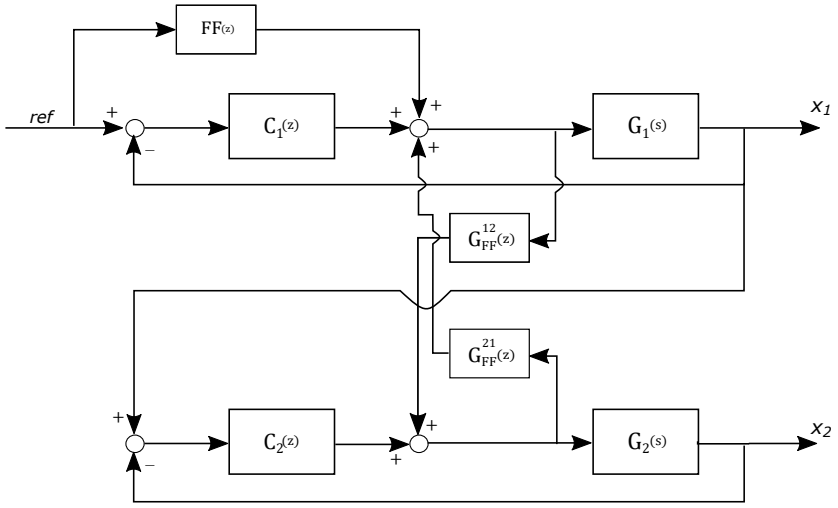

Figure 7.3: Block diagram of the control structure used for dual stage reference tracking. The master/slave control scheme is added with decoupling and reference feedforward.

A fourth order reference profile was generated as explained in section 6.1. The parameters used to generate the trajectory are listed in Table 7.1

Parameter	Value
Displacement	3 mm
Maximum velocity	$2\,\mathrm{cm\,s^{-1}}$
Maximum acceleration	$0.25\,\mathrm{m/s^2}$
Maximum jerk	$50\,\mathrm{m/s^3}$
Maximum snap	$500\,\mathrm{m/s^4}$

Table 7.1: Amplitude and the constraints on the derivatives of the fourth order profile

The coarse stage was controlled by a PID with a bandwidth of 70 Hz and the fine stage is controlled by each of the controllers designed for the fine stage. The obtained tracking errors when using the reset controllers are compared with that of PID in Figure 7.4. It can be seen that controller A performs better than PID, and the RMS error has been calculated to have reduced by 50.6 %. Controller B provides better tracking that controller A, as expected, and RMS error reduced by 61.7 %. Performance of controller C was similar to that of PID.

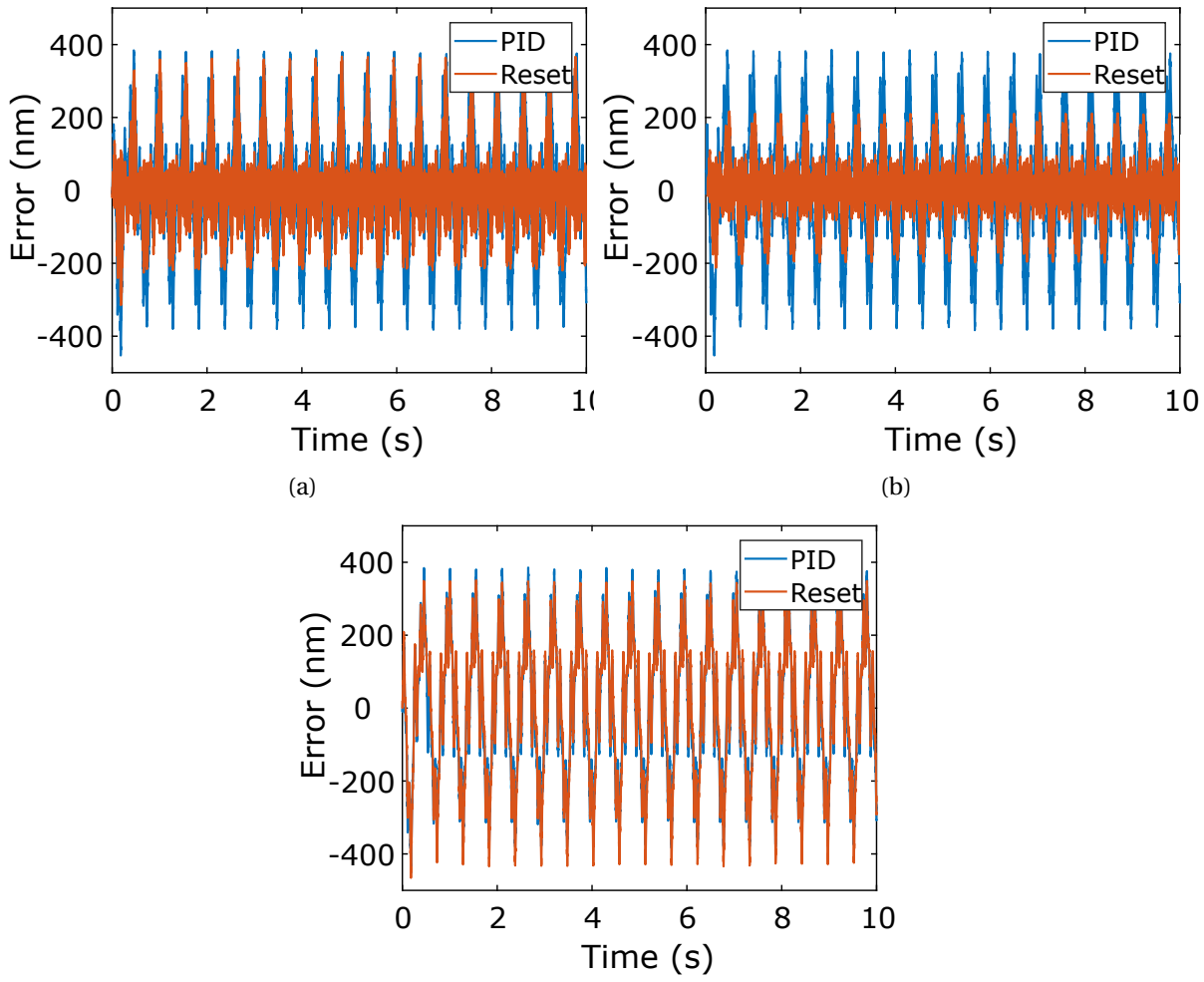

(a)

(b)

(c)

Figure 7.4: (a) Case 1 -Tracking error for Reset controller A vs PID. (b) Case 2 - Tracking error for Reset controller B vs PID. (c) Case 3 - Tracking error for Reset controller C vs PID.

8

GUIDELINES FOR TUNING

In this chapter, basic rules of thumb that can be used to tune the three developed controllers are provided. Controller parameters largely depend on the phase margin required and the value of γ to be used, and therefore can not be generalized. Guidelines provided are for the case $\gamma = 0$.

8.1. RESET CONTROLLERS A AND B

- Integral action is terminated at $\omega_i = \omega_c/10$.
- Differentiating action is started at $\omega_d = \omega_c/5$.
- Taming pole of lead component is placed at $\omega_t = \alpha\omega_d$ where $\alpha = 0.75$.
- The corner frequency for LPF is taken as $\omega_l = 7 \times \omega_c$.
- For Controller A, the proportional gain is equal to the inverse of the gain of the plant at ω_c.
- For Controller B, the proportional gain is 1.75 times the inverse of the gain of the plant at ω_c.

8.2. RESET CONTROLLER C

- Differentiating action is started at $\omega_d = \omega_c/3$ and terminated at $\omega_t = \omega_c \times 3$.
- Integral action is terminated at $\omega_i = \omega_c/10$.
- Proportional gain is calculated by taking the inverse gain of the plant transfer function at ω_c and dividing by 3.
- Corner frequency of reset LPF is placed at $\omega_{lr} = 4.5 \times \omega_c$ to achieve the same phase margin obtained when using a linear LPF at $\omega_l = 6 \times \omega_c$.

9

CONCLUSIONS

9.1. GENERAL CONCLUSIONS

In this thesis, reset control has been implemented in the PID control scheme with the view of relaxing the waterbed effect, and improving the bandwidth of the system while maintaining the same level of precision, and vice versa. New design rules for Reset PID control have been developed, analogous to the rules of thumb used for tuning PID controllers.

Describing function analysis was used as an approximation method to aid in the loop shaping process, while developing reset controllers. Three different controller configurations are used; two configurations with reset implemented in the taming pole of the lead component, and one configuration with reset in the low pass filter. The first configuration termed 'Reset Controller A' provides improvement in precision and tracking while maintaining the same bandwidth and phase margin compared to linear PID. 'Reset Controller B' has been tuned to provide better tracking and higher bandwidth while maintaining same precision and phase margin. The tracking performance of controller B is better than that of controller A. 'Reset Controller C', with reset in LPF, provides improvement in precision while all other performance criteria are the same.

The controllers have been shown to satisfy sufficient conditions for ensuring asymptotic stability. The controllers are then implemented digitally within a MATLAB/Simulink environment and implemented on a dual stage positioning system, via a real-time dSPACE DS1103 controller interface. A toolbox has been created that can be used for implementation of Reset PID and for further research. The fine stage was separated from the coarse stage and mounted to the optical test facility for initial experiments to validate the developed controllers. Time domain experiments were conducted on the fine stage to study the performance with regard to tracking and precision. In the frequency domain, closed loop identification techniques were used to identify the complementary sensitivity and sensitivity functions.

A fourth order input-shaped reference signal with a stroke of 400 nm was applied to the

closed loop system along with second order feedforward. The tracking errors from using each of the three reset controllers were compared with the tracking error from PID. It was observed that controller A provided the best tracking performance, with an RMS error that is 56 % of that of PID. Controller B provided further improvement in tracking, and the RMS error reduced to 39 % of that of PID. This is inline with the open loop shapes obtained by describing function analysis. The tracking performance of controller C showed no improvement over PID.

The steady state precision of the 3 reset controllers and PID were measured to be 10 nm, which is the same as the resolution of the interferometer used. In order to study the improvement in precision, a 50 nm white noise signal was added as measurement noise in the closed loop, while the reference was set at zero. The PID controller produced a maximum steady state error of 40 nm, while this was reduced to 20 nm for controller A and 30 nm for controller C. Controllers A and C were tuned to provided better precision at the same bandwidth as the PID at 150 Hz, and it is seen that both controllers have achieved that, with controller A performing better than controller C. Thus, controller A can be chosen to be the better choice, also noting that it provides better tracking than controller C. Reset Controller B with bandwidth at 200 Hz provided the same precision as the PID with bandwidth 150 Hz which is a 33 % improvement in bandwidth.

The measured closed loop frequency responses were compared with those calculated from describing functions and it was observed that they match well. It was shown that though the phase added by reset lead element is slightly lesser than expected for controllers A and B, describing functions provide a good approximation of phase addition in Reset PID. For controller C, the improvement in precision was substantiated by the reduced complementary sensitivity function at high frequencies.

A fourth order reference profile with a stroke of 3 cm was then applied to the dual stage system with fourth order feedforward. The two stages were decoupled from each other using additional feedforward, so as to minimize the effect of one closed loop on another. The coarse stage was controlled by a PID controller of bandwidth 70 Hz, while the fine stage was controlled by the same controllers as before. Controller A provided a reduction of around 51 % in tracking error, while it was around 62 % for controller B. This is in line with the performance obtained from the second order system.

The water-bed effect, due to which it was impossible to improve bandwidth or precision without impacting the other was impossible in PID has been overcome to a considerable extent using reset control. The reset controllers, as explained above have shown better precision without compromising the bandwidth and higher bandwidth without reduction in precision.

9.2. RECOMMENDATIONS

During the course of the thesis, several observations were made that can further enhance the knowledge behind Reset PID control. Also, more general recommendations are given that would help understand reset control better.

9.2.1. HIGHER ORDER DESCRIBING FUNCTION ANALYSIS

The sinusoidal input describing method used in this thesis only considers the first coefficient of the fourier transform of output. This method thus ignores the higher order dynamics induced by reset. Although the practical results from the setup correspond well to the simulated results, taking into consideration the higher order dynamics can help understand the effects of increasing nonlinearity on the system. A detailed approach for Higher Order Describing Function Analysis (HOSIDF) can be found in [20], and this could be implemented in future work.

9.2.2. PHASE ADDITION BY RESET

It was observed that the sensitivity peak for controller A and B were slightly larger in practice than what was estimated from describing functions. Further study is required to ascertain the cause for this.

9.2.3. DISTURBANCE REJECTION

This thesis was intended to overcome the waterbed effect in PID control, with focus on achieving better bandwidth and precision independently without affecting each other. The performance of Reset PID controllers have not been analyzed from the point of view of disturbance rejection. It has been shown in [7] that adding phase to the system through reset without affecting the gain characteristics can help achieve mid-frequency disturbance rejection. In Reset controllers A and B, the amount of phase added can be changed by changing the nonlinearity in the system, without affecting the gain behavior. The performance however needs to be validated.

9.2.4. STEP RESPONSE

Although all the controllers in the thesis have been made to have the same phase margin as the PID controller against which the comparisons are made, step response of the system was not studied. Analyzing step response can help understand the relationship between the describing function phase margin and overshoot in reset systems.

9.2.5. DOUBLE RESET

Reset has been implemented in the lead component and low pass filter individually. Further research is necessary to check if precision can be improved by applying reset in both components simultaneously.Implementation will be less straight-forward because unlike

with linear control elements, positions of the reset elements in the control loop do affect the response of the system. Design complexity increases when different γ values need to be used for the two reset elements and new rules of thumb will have to be defined.

BIBLIOGRAPHY

[1] M. Iwasaki, K. Seki, and Y. Maeda, *High-precision motion control techniques: A promising approach to improving motion performance,* IEEE Industrial Electronics Magazine **6**, 32 (2012).

[2] R. Schmidt, G. Schitter, and A. Rankers, *The Design of High Performance Mechatronics - 2nd Revised Edition: High-Tech Functionality by Multidisciplinary System Integration*, EBL-Schweitzer (IOS Press, 2014).

[3] K. Åström, *Limitations on control system performance,* European Journal of Control **6**, 2 (2000).

[4] M. M. Seron, G. C. Goodwin, and J. Braslavsky, *Fundamental Limitations in Filtering Control*, 1st ed. (Springer-Verlag New York, Inc., Secaucus, NJ, USA, 1997).

[5] A. Baos and A. Barreiro, *Reset Control Systems* (Springer Publishing Company, Incorporated, 2013).

[6] I. HOROWITZ and P. ROSENBAUMâ€ , *Non-linear design for cost of feedback reduction in systems with large parameter uncertainty,* International Journal of Control **21**, 977 (1975), http://dx.doi.org/10.1080/00207177508922051 .

[7] Y. Guo, Y. Wang, and L. Xie, *Frequency-domain properties of reset systems with application in hard-disk-drive systems,* IEEE Transactions on Control Systems Technology **17**, 1446 (2009).

[8] H. Hosseinnia, I. Tejado, and B. Vinagre, *Fractional-order reset control: Application to a servomotor, Mechatronics*, **23**, 781–788 (2013).

[9] O. Beker, C. V. Hollot, and Y. Chait, *Plant with integrator: an example of reset control overcoming limitations of linear feedback,* IEEE Transactions on Automatic Control **46**, 1797 (2001).

[10] Y. Li, G. Guo, and Y. Wang, *Phase lead reset control design with an application to hdd servo systems,* in *2006 9th International Conference on Control, Automation, Robotics and Vision* (2006) pp. 1–6.

[11] Y. QianChen and C.V.Hollot, *Analysis of reset control systems consisting of a fore and second-order loop, ASME Journal of Dynamic Systems, Measurement and Control*, (2000).

[12] N. Saikumar and H. Hosseinnia, *Generalized fractional order reset element (gfrore),* (2017).

[13] A. Gelb and W. E. Vander Velde, *Multiple-input describing functions and nonlinear system design* (New York : McGraw-Hill, 1968) includes bibliographies.

[14] J. C. Clegg, *A nonlinear integrator for servomechanisms,* Transactions of the American Institute of Electrical Engineers, Part II: Applications and Industry **77**, 41 (1958).

[15] L. Hazeleger, M. Heertjes, and H. Nijmeijer, *Second-order reset elements for stage control design,* in *2016 American Control Conference (ACC)* (2016) pp. 2643–2648.

[16] B. Joziasse, *Nanometer precision scanning dual stage with reduced Joule heating in the fine stage actuator,* Master's thesis, Delft University of Technology, The Netherlands (2017).

[17] P. Lambrechts, M. Boerlage, and M. Steinbuch, *Trajectory planning and feedforward design for electromechanical motion systems, Control Engineering Practice,* **13**, 145 (2005).

[18] D. Nesic, A. R. Teel, and L. Zaccarian, *Stability and performance of siso control systems with first-order reset elements,* IEEE Transactions on Automatic Control **56**, 2567 (2011).

[19] G. A. Dumont, *Decoupling control of mimo systems,* (2011).

[20] P. Nuij, O. Bosgra, and M. Steinbuch, *Higher-order sinusoidal input describing functions for the analysis of non-linear systems with harmonic responses,* Mechanical Systems and Signal Processing **20**, 1883 (2006).

A

DATASHEETS

In this section, the data sheets of the Aerotech ABL101000LT linear stage and Aerotech Soloist ML motion composer can be found.

A.1. AEROTECH ABL10100LT

ABL1000 Series SPECIFICATIONS

Basic Model		ABL1000			
Total Travel		25 mm	50 mm	100 mm	150 mm
Drive System		Linear Brushless Servomotor			
Bus Voltage		80 VDC			
Continuous Current	A_{pk}	up to 2.9 A			
	A_{rms}	up to 2.1 A			
BEMF, line-line, max.	V/m/sec	3.77952			
	V/in/sec	0.096			
Force Constant, Sinusoidal Drive	N/A (lb/A), pk	3.29 (0.739)			
	N/A (lb/A), rms	4.65 (1.04)			
Resistance, 25 C, line-line	Ohms	5.2			
Resistance, 125 C, line-line	Ohms	7.28			
Inductance, line-line	mH	0.7			
Magnetic Pole Pitch	mm (inch)	16 (0.63)			
Feedback		Noncontact Linear Encoder			
Resolution	LN	0.5 nm (0.02 µin)			
	LT	2.5 nm (0.1 µin)			
Maximum Travel Speed[1]		300 mm/s (12 in/s)			
Maximum Linear Acceleration		1 g - 10 m/s² (394 in/s²)(no load)			
Maximum Load[2]	Horizontal	15.0 kg (33.0 lb)			
Accuracy	LN	±0.2 µm (±8 µin)[3,4] ±1 µm (±40 µin)	±0.2 µm (±8 µin)[3,4] ±1 µm (±40 µin)	±0.2 µm (±8 µin)[3,4] ±2 µm (±80 µin)	±0.5 µm (±20 µin)[3,4] ±3 µm (±120 µin)
	LT	±0.3 µm (±12 µin)[3,4] ±2 µm (±80 µin)	±0.3 µm (±12 µin)[3,4] ±2 µm (±80 µin)	±0.3 µm (±12 µin)[3,4] ±5 µm (±200 µin)	±0.5 µm (±20 µin)[3,4] ±5 µm (±200 µin)
Repeatability	LN[3]	±50 nm (±2 µin)			
	LT	±50 nm (±2 µin)[3]; ±100 nm (±4 µin)			
Straightness and Flatness[4]		±0.25 µm (±10 µin)	±0.25 µm (±10 µin)	±0.4 µm (±16 µin)	±0.4 µm (±16 µin)
Pitch and Yaw		±0.25 arc sec	±0.50 arc sec	±1.0 arc sec	±1.5 arc sec
Nominal Stage Weight		4.5 kg (10 lb)	5.5 kg (12 lb)	6.4 kg (14 lb)	12.7 kg (28 lb)
Moving Mass		1.9 kg (4.2 lb)			4.8 kg (10.6 lb)
Operating Pressure[5]		80 psi ±5 psi			
Air Consumption[5,6,7]		17.5 SLPM	17.5 SLPM	17.5 SLPM	13.2 SLPM
Construction		Aluminum Body/Hardcoat			

Notes:
1. Maximum speed based on stage capability; maximum application velocity may be limited by system data rate and system resolution.
2. Max load for XY configuration is 10.0 kg
3. Values with Aerotech controls and HAL option.
4. Dependent on flatness of stage mounting surface.
5. To protect air bearing against under-pressure, an in-line pressure switch tied to the controller E-stop input is required.
6. Air supply must be clean, dry to 0° F dew point, and filtered to 0.25 µm or better; recommend nitrogen at 99.99% purity.
7. Maximum expected air consumption for single axis.
8. ABL10150 must be used as the bottom axis of an XY stack.
9. Specifications are for single-axis systems, measured 25 mm above the tabletop. Performance of multi-axis systems is payload and workpoint dependent. Consult factory for multi-axis or non-standard applications.

WORLD HEADQUARTERS: Aerotech, Inc., United States • Phone: +1-412.963.7470 • Email: sales@aerotech.com
Aerotech, Ltd., United Kingdom • Phone: +44.118.940.9400 • Email: sales@aerotech.co.uk
Aerotech GmbH, Germany • Phone: +49.911.967.9370 • Email: sales@aerotechgmbh.de
Aerotech KK, Japan • Phone: +81.47.489.1741 • Email: sales@aerotechkk.co.jp
Aerotech China • Phone: +852.3793.3488 • Email: saleschina@aerotech.com

ABL1000 Series DIMENSIONS

ABL10025/50/100 Single-Axis Configuration

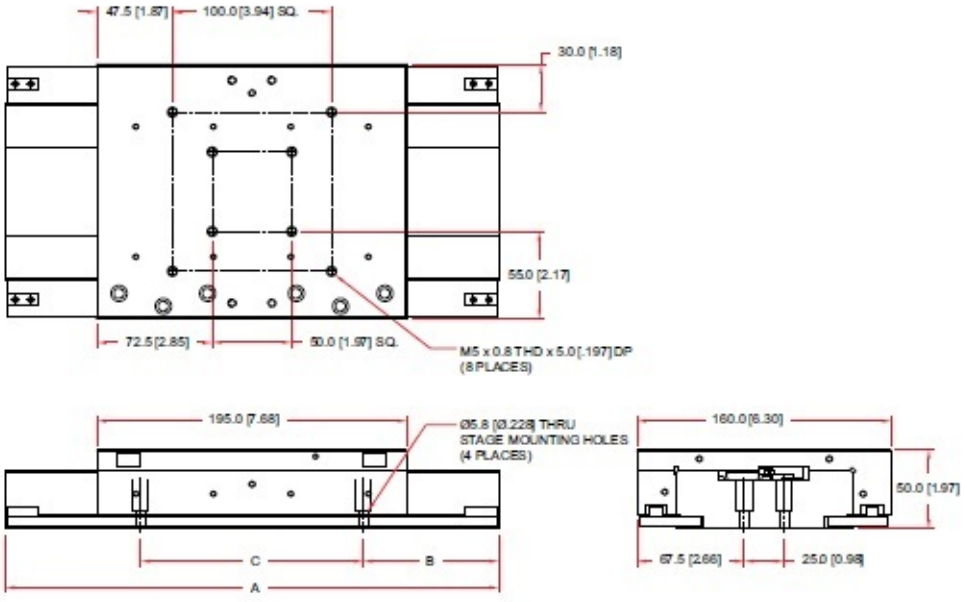

Basic Model	Total Travel	Dimensions - Millimeters [Inches]		
		A	B	C
ABL10025	25.0 [1.00]	235.0 [9.25]	35.0 [1.38]	165.0 [6.49]
ABL10050	50.0 [2.00]	260.0 [10.24]	60.0 [2.36]	140.0 [5.51]
ABL10100	100.0 [4.00]	310.0 [12.20]	85.0 [3.35]	140.0 [5.51]

A.2. AEROTECH SOLOIST ML

Soloist ML SPECIFICATIONS

Soloist ML	Units	
Motor Style		Brush, Brushless, Stepper, Voice Coil
Motor Supply	VAC	±40 max
Control Supply[1]	VAC	18-36 VDC
Bus Voltage[2]	VDC	±40
Peak Output Current (1 sec)[3,4]	A_{pk}	10
Continuous Output Current[3,4]	A_{pk}	5
Digital Inputs		N/A
Digital Outputs		N/A
Analog Inputs		One 16-bit Differential; ±10 V
Analog Outputs		N/A
Dedicated Axis I/O on Feedback Connector		Three Limit Inputs (CW, CCW, Home); Three Hall Effect Inputs (A, B, C); Three High-Speed differential Inputs (sin, cos, mkr for encoder); Motor Over-Temperature Input
Dedicated I/O on Auxiliary Feedback Connector		sin, cos, mkr for Aux Enc; Aux Enc can be used for PSO Output
I/O Expansion Board[5]		8/8 Digital Opto-Isolated; 1 Analog In (±10 V, 16-bit Differential); 1 Analog Out (±5 V, 16-bit)
High Speed Data Capture		Yes (50 ns Latency)
Automatic Brake Control		Optional
Emergency Stop Sense Input (ESTOP)[6]		Standard; 24 V Opto-Isolated
Position Synchronized Output (PSO)		Single Axis Only
Can Output Multiplied Encoder		Yes (MXH Only)
Can Output Square Wave Encoder		Yes
Primary Encoder Input Frequency		32 MHz Square Wave Standard; 2 MHz Sine Wave (MXU or MXH)
Secondary Encoder Input Frequency		32 MHz Square Wave
Encoder Multiplication		Up to x4096 (MXU); Up to x65536 with Quadrature Output (MXH)
Resolver Interface		N/A
Internal Shunt Resistor		N/A
External Shunt		N/A
Ethernet		Yes
USB		No
RS-232		Yes
FireWire		No
Fieldbus		Modbus TCP; Ethernet/IP
Current Loop Update Rate	kHz	20
Servo Loop Update Rate	kHz	10
Power Amplifier Bandwidth	kHz	Selectable Through Software
Minimum Load Inductance	mH	0
Operating Temperature	°C	0 to 50
Storage Temperature	°C	-30 to 85
Weight	kg (lb)	0.45 (1.0)
Standards		CE approved, NRTL safety certification, 2011/65/EU RoHS 2 Directive

Notes:
1. "Keep Alive" supply.
2. Output voltage dependent upon input voltage.
3. Peak value of the sine wave; rms current for AC motors is 0.707 * A_{pk}.
4. Load dependent.
5. Requires I/O option.
6. Requires external relay to remove motor supply power.

Soloist ML DIMENSIONS

Soloist ML with additional I/O
(Dimensions without optional I/O are identical)

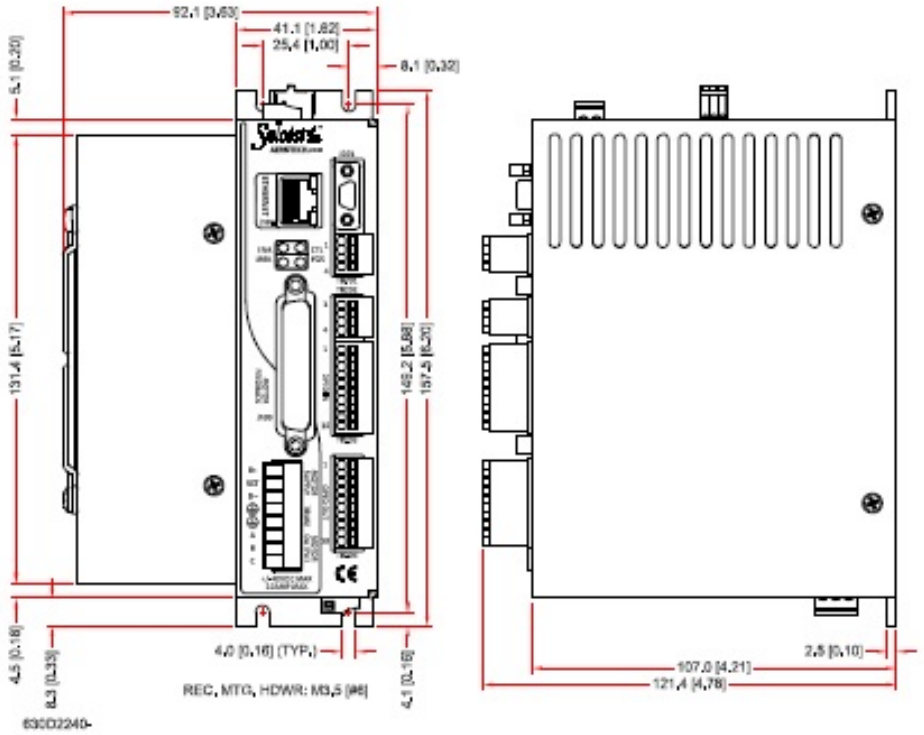

Soloist Ordering Information

Visit Aerotech's website for complete ordering information.

B

FINE STAGE SPECIFICATIONS

B.1. ACTUATOR SPECIFICATIONS

Specification	Value
Resistance R	2.1 Ω
Inductance L	580 µH
No. of windings	140
Coil dimensions	30 × 60 × 2 mm
Magnet dimensions	20 × 6 × 3 mm
Magnet remanent flux density B_r	1.42 T
Average flux density in air gap B_g	0.85 T
Motor constant	1.61 NA^{-1}

B.2. AMPLIFIER SPECIFICATIONS

Specification	Value
Gain (A/V)	0.348
Offset (mA)	0.5
Noise level at 10 kHz (mA_{pp})	6

C

MATLAB CODE - STABILITY CHECK

C.1. LYAPUNOV STABILITY

```
%
    ------------------------------------------------------------------------

%   Check Hbeta stability condition
%
    ------------------------------------------------------------------------


%Plant TF
load Hindividual
P_tf = H2;

%% Compute Reset PID controller

% Initialise parameters

PM = 45;
BW = 150; % Bandwidth in Hz
mode = 'RCA'; % mode -   string, 'RCA' for Reset Controller A,
              %                 'RCB' for Reset Controller B,
              %                 'RCC' for Reset Controller C

%function call to calculate controller
[ss_rc,Arho, nr] = resetgen_s(mode,P_tf,PM,BW);

%% Initialise LMI
% Compute closed loop system

syscl=feedback(series(ss_rc,ss(P_tf)),1);
```

```
Acl=syscl.a;    % Closed loop A-matrix
A=Acl/norm(Acl); % Normalise A-matrix

nnr = size(ss_rc.a,1)-nr;
np = order(P_tf);

% Compute C0 and B0
Cp=ss(H2).c;
beta=sdpvar(1,1,'full','real'); % sdpvar - symbolic decision variable
Prho=sdpvar(1,1,'full','real');

B0=[zeros(np,nr);zeros(nnr,nr);ones(nr,nr)];
C0=[beta*Cp zeros(nr,nnr) Prho];
P=sdpvar(size(syscl.a,1),size(syscl.a,1),'symmetric');

%% Solve LMI
% Requires installation of YALMIP

lmi=A'*P+P*A<=0;
eps=1e-14;
constr=[P>=eps*eye(size(syscl.a,1)), B0'*P==C0];
ops=sdpsettings('solver','sedumi','verbose',0,'debug',1);

F=solvesdp([lmi constr],0,ops);

if F.problem==0
    display(strcat('Solution found'))
end
```

C.2. GLOBAL ASYMPTOTIC STABILITY

```
%
    ------------------------------------------------------------------------

% |lambda(Arho*exp(pi/w*Aol)|
%
    ------------------------------------------------------------------------


%Plant TF
load Hindividual
P_tf = H2;

%% Compute Reset PID controller

% Initialise parameters
f=logspace(1,6,1e3);
```

```
PM = 45;      % Phase margin
BW = 150;     % Bandwidth in Hz
mode = 'RCA';% mode - string, 'RCA' for Reset Controller A,
              %               'RCB' for Reset Controller B,
              %               'RCC' for Reset Controller C

%function call to calculate controller
[ss_rc,Arho, nr] = resetgen_s(mode, P_tf,PM,BW);

%% Compute open-loop

P=ss(P_tf);
L=series(ss_rc,P);

n=size(ss_rc.a,1); % number of controller states
m=size(P.a,1); % number of plant states

%% Compute and plot eigenvalues
eigenval=zeros(n+m); % initialize

Arho = blkdiag(Arho, eye(m));

for i=1:length(f);
 w=2*pi*f(i);
 term=Arho*(expm(pi/w*L.a));
 if sum(sum(isnan(term)))==0;
  eigenval(:,i)=abs(eig(term));
 end
end

 semilogx(f,eigenval)
 hold on
ylabel('$|\lambda(A_\rho e^{\frac{\pi}{\omega} A_{ol}})|$')
 xlabel('Frequency (Hz)')
 grid on
set(gca,'YMinorTick','on')
```

No more differentiator in PID: Development of Nonlinear PID Control for Motion Systems

A. Palanikumar, N. Saikumar, S. Hassan HosseinNia

Abstract— **Industrial PID consist of three elements, Lag, Lead and Low Pass Filters (LPF). PID being a linear control method is inherently bounded by the waterbed effect due to which there exists a trade-off between precision and tracking, provided by Lag and LPF on one side and stability and robustness, provided by Lead, on the other side. Nonlinear reset strategies applied in the Lag and LPF elements have been very effective in reducing this trade. However, there is lack of study in developing a reset Lead element. In this paper, we develop a novel lead element which provides higher precision and stability unlike the linear lead filters. The concept is presented and validated on a Lorentz-actuated nanometer precision stage. Improving the precision, tracking and bandwidth are shown through two separate designs. The performance is validated in both time and frequency domain to ensure that phase margin achieved on the practical setup matches design theories.**

I. INTRODUCTION

The high tech industry is at the forefront of pushing the limitations and barriers in motion control technology. Demands for achieving higher precision and speeds are ever increasing. The wafer scanner industry, which is involved in manufacturing integrated circuits, is a prime example where (sub) nanometer precision positioning is required, while at the same time meeting challenging throughput demands. For accurate and fast servo-positioning of mechanical actuators in real life engineering systems, high quality motion control is required.

PID and related linear controllers (includes use of other linear filters) have been the standard for industrial motion control for many years owing to various factors such as its wide applicability and ease of implementation. PID does not require a precise model or thorough knowledge of the system and can instead be tuned using standard guidelines. With multiple advancements in feedforward control techniques, it has become possible to achieve high bandwidths and precision using PID. However, when extreme demands have to be met, the fundamental limitations of linear control, to which PID is not exempt, become more evident. Such inherent limitations cause different performance criteria to be conflicting in nature, making it impossible to improve one criterion without negatively influencing another. This phenomenon is known in linear control theory as waterbed effect. For a more detailed explanation of the water bed effect, [1] and [2] can be referred.

The authors are with the Department of Precision and Microsystems Engineering, Delft University of Technology, Delft, The Netherlands

Requirements for precision motion control have been discussed in detail in [3] and [4]. Loop shaping, one of the popular methods for designing PID controllers in the high tech industry, is a technique in which the controller is designed in such a way that the frequency response of the open loop transfer function has the desired shape in gain and phase. For good tracking, high gain at frequencies upto the bandwidth is required. In PID, the integrator plays the role of increasing gain at low frequencies. Simultaneously, gain at high frequencies needs to be low to effectively attenuate noise in the system and hence provide good precision. This is commonly achieved through the use of low pass filters. In the frequency region around the bandwidth, phase behavior determines the stability and robustness of the system . Phase addition in PID is achieved by the tamed differentiator or lead component. The constraint in the relation between gain and phase behavior in linear systems is explained by Bode's gain-phase relationship [5]. Hence attempts to change gain behaviour to improve precision and/or tracking negatively affects phase and hence stability and vice-versa. Also attempts to improve bandwidth results in decrease in phase margin and deterioration in precision performance. These limitations are fundamental to linear controllers including advanced optimal linear control and can only be overcome with the use of nonlinear control.

Reset control is one such promising technique which can be used for this purpose. Reset control was first introduced by J.C. Clegg in 1958, in the form of an integrator whose state is reset whenever the input error signal crosses zero [6]. Approximation of the behavior of Clegg integrator (CI) through describing function analysis shows that the CI has a phase lag of about -38°, which is 52° higher than that of a linear integrator, for similar gain behavior. Since then, a lot of work has been done on reset control theory and the benefits of using reset controllers in various practical applications have been investigated. For example, reset control has been used to achieve improved performance in hard-disk-drive systems, [7], [8] and mechatronic systems [9], [10]. In [11], it is shown that reset can be used to reduce overshoot and improve settling time in PZT positioning stages. Despite the promise shown, it is observed that much of the research in reset control was focused on the integrator. Some efforts have been made in investigating other reset elements as well. For example, in [12], a generalized fractional order reset element is introduced. In [13], a reset lead-lag filter has been used to improve mid-frequency disturbance rejection. And in [14], a second

order reset element has been introduced to be used in stage control design. However apart from reset integrator, the use of reset elements within the framework of PID for improved performance has not been well investigated.

The motivation for this research arises from the possibility of reducing the severity of the waterbed effect limitation in PID using reset control. In this paper, reset has been implemented in the taming pole of the lead component in PID, and a Reset PID controller has been developed using common loop shaping techniques. The main contribution of this work is the concept of reset PID to overcome fundamental limitations of linear control along with two cases of reset PID controller design with first design used to improve tracking and precision for same bandwidth and second design for increase in bandwidth and tracking for same precision.

In section II, necessary background information about reset control is provided. The concept of reset PID is provided in section III. The experimental setup used for validation of the developed controllers is described in section IV. In section V, experimental results from implementation of the two controllers are given, and compared with the performance of linear PID controller, followed by conclusions.

II. PRELIMINARIES

A. Definition of Reset Control

A general reset controller can be defined as follows, using the notations used in [1]:

$$\Sigma_{RC} := \begin{cases} \dot{x}_r(t) = A_R x_r(t) + B_R e(t) & \text{if } e(t) \neq 0, \\ x_r(t^+) = A_\rho x_r(t) & \text{if } e(t) = 0 \\ u(t) = C_R x_r(t) + D_R e(t) \end{cases} \quad (1)$$

where matrices A_R, B_R, C_R, D_R are the base linear state-space matrices of the control system. A_ρ is the reset matrix, which determines the after reset values of the states. $u(t)$ is the control input and the error signal $e(t)$ is the difference between reference $r(t)$ and output $y(t)$. $x_r(t)$ denotes the controller states. A typical control structure using reset control is shown in Fig. 1. The reset controller Σ_{RC} is separated into two components : a nonlinear part Σ_r whose states are reset, and a linear part Σ_{nr} whose states are not reset. The two components are connected in series, with the output $u_r(t)$ from reset part given as input to the non reset part.

B. Describing Function Analysis

Frequency response of reset elements can be approximated using describing function analysis. This method makes the assumption that non linear system behavior has a quasi-linear amplitude dependent relation between sinusoidal excitation inputs and the steady state response at the fundamental excitation frequency. The higher harmonics are neglected under the assumption that they are sufficiently

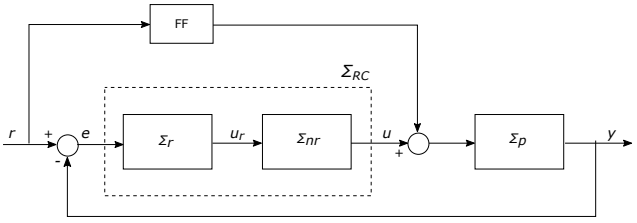

Fig. 1: Block diagram of feedback loop with a reset controller Σ_{RC}, and plant Σ_p. Feedforward term FF is calculated as given in [15].

filtered out by the low pass characteristics of the system. Describing functions thus help extend the use of loop shaping techniques to reset control. For a more detailed explanation of describing functions, [16] can be referred.

The general describing function of a reset system as defined in [7] is given by:

$$G_{\mathrm{DF}}(j\omega) = C_R(j\omega I - A_R)^{-1}B_R(I + j\Theta_D(\omega)) + D_R \quad (2)$$

with

$$\Theta_D(\omega) = -\frac{2\omega^2}{\pi}\Delta(\omega)[\Gamma_D(\omega) - \Lambda^{-1}(\omega)] \quad (3)$$

where the following equations have been used:

$$\begin{cases} \Lambda(\omega) = \omega^2 I + A_R^2 \\ \Delta(\omega) = I + e^{\frac{\pi}{\omega}A_R} \\ \Delta_D(\omega) = I + A_\rho e^{\frac{\pi}{\omega}A_R} \end{cases}$$

C. Controlling nonlinearity with γ

The reset matrix A_ρ in (1) provides a degree of freedom in tuning the system and is defined as follows:

$$A_\rho = \begin{bmatrix} \gamma I_{n_r} & 0 \\ 0 & I_{n_{nr}} \end{bmatrix} \quad (4)$$

where n_r and n_{nr} are the number of states in Σ_r and Σ_{nr} respectively.

If the resetting parameter $\gamma = 1$, the reset element reduces to its base linear system as no reset occurs and $\gamma = -1$ denotes extreme reset. As $|\gamma - 1|$ increases, the nonlinearity in the system increases because the magnitude of jump in state value increases. Increase in nonlinearity is not desired due to the associated higher order dynamics. The variation of phase lag with change in γ is shown in Fig. 2a, and it can be seen that the more nonlinear the system is, greater is the phase benefit.

Describing function of the generalized first order reset element (GFORE) developed in [7], is compared with a linear lag filter in Fig. 3. It can be seen that for the case of $\gamma = 0$, upto the corner frequency at $100\,\mathrm{Hz}$, the behavior of GFORE is similar to that of the lag filter. At higher frequencies, the phase lag in GFORE is only 38° (for $A_\rho = 0$), as compared to 90° in lag filter, while gain behaviors are almost similar. Describing functions have also been plotted for $\gamma = -0.5$

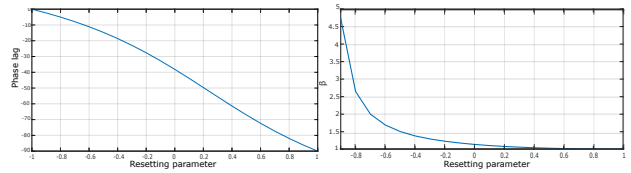

(a) (b)

Fig. 2: (a) Variation of phase lag with change in γ.(b)Variation of ratio β with change in γ.

and $\gamma = 0.5$ to depict the variation in frequency response with changing γ.

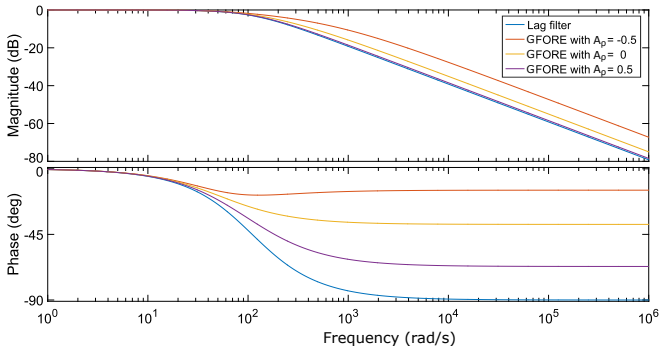

Fig. 3: Frequency response of FORE compared with that of a linear lag filter.

It can be seen that the cutoff frequency of GFORE also varies with change in γ [12]. The ratio of cutoff frequency of GFORE to that of lag filter (β) is plotted in Fig. 2b for different values of γ . Choosing γ values between -1 and 1 can help attain the desired trade-off between phase lag, cutoff frequency and non linearity.

D. Stability Analysis

The stability condition given in [1] is used for checking the stability of the system. The following condition was provided for ensuring asymptotic stability of a reset control system :

Theorem [1] *There exists a constant* $\beta \in \mathbb{R}^{n_r \times 1}$ *and* $P_\rho \in \mathbb{R}^{n_r \times n_r}, P_\rho > 0$ *where* n_r *is the number of reset states, such that the restricted Lyapunov equation*

$$P > 0, \;\; A_{cl}^T P + P A_{cl} < 0 \tag{5}$$

$$B_0^T P = C_0 \tag{6}$$

has a solution for P*, where* C_0 *and* B_0 *are defined by*

$$C_0 = \begin{bmatrix} \beta C_{nrp} & 0_{n_r \times n_{nr}} & P_\rho \end{bmatrix}, \quad B_0 = \begin{bmatrix} 0_{n_{nrp} \times n_r} \\ 0_{n_r \times n_r} \\ I_{n_r} \end{bmatrix} \tag{7}$$

A_{cl} is the closed loop matrix A-matrix

$$C_0 = \begin{bmatrix} A_r & B_r C_{nrp} \\ -B_{nrp} C_r & A_{nrp} \end{bmatrix} \tag{8}$$

in which (A_r, B_r, C_r, D_r) are the state space matrices of Σ_r and $(A_{nrp}, B_{nrp}, C_{nrp}, D_{nrp})$ are the state space matrices of Σ_{nr} and Σ_p in series.

This condition has been used to test stability of all developed controllers.

III. RESET PID

Transfer function of linear PID in series form is given by:

$$G_{PID} = K_p \underbrace{\left(1 + \frac{\omega_I}{s}\right)}_{\text{Lag component}} \underbrace{\left(\frac{s}{\omega_d} + 1\right) \Big/ \left(\frac{s}{\omega_t} + 1\right)}_{\text{Lead component}} \underbrace{\left(\frac{\omega_l}{s + \omega_l}\right)}_{\text{LPF}} \tag{9}$$

where ω_I is the frequency at which integral action is stopped, and ω_l is the cut off frequency of the LPF. K_p is the proportional gain. Differentiating action is started at ω_d and terminated at ω_t, and therefore $\omega_t > \omega_d$.

As discussed in section I, differentiator or lead component of the PID adds essential phase to the system in bandwidth region to achieve stability and robustness. Phase at the crossover frequency also affects the maximum overshoot of the system. Differentiator is tamed by placing a pole at ω_t because having large gains at higher frequencies is not desirable for noise attenuation and precision. The maximum phase lead that can be achieved from the differentiator in the absence of this taming pole would be $90°$. However, the pole reduces the maximum phase lead to a value which depends on frequency interval between the zero and the pole. By symmetrically placing the zero and pole around the crossover frequency ω_c, it is ensured that the maximum phase from lead is achieved at bandwidth. Fig. 4a shows the frequency response of a typical differentiator used in PID.

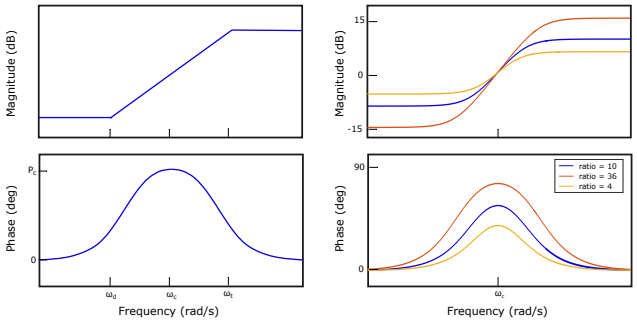

(a) (b)

Fig. 4: (a) Bode plot of a differentiator. (b) Bode plot showing increase in maximum phase and also high freqeuncy gain with increasing ratio of ω_t to ω_d

Higher and lower phase margins can be achieved by increasing or decreasing the frequency range between ω_d and ω_t respectively. The problem with this approach is that it results in a trade-off between tracking and precision performance on one side and stability and robustness on the other. This can be observed in Fig. 4b. As the positive phase obtained increases with increase in the ratio of ω_t to ω_d, the gain at higher frequencies is also increased, which affects the precision of the system. As a result, with the linear design, it is not possible to improve precision while having the same degree of robustness. Also, with increasing phase, there is a decrease in low frequency gain thereby affecting tracking behavior.

Reset can be introduced in this tamed differentiator to improve performance such that this fundamental limitation is overcome. Reset is introduced such that only the taming pole is reset resulting in the reset and non-reset parts given by:

$$\Sigma_{nr} = \left(\frac{s}{\omega_d} + 1\right); \quad \Sigma_r = \frac{1}{\left(\frac{s}{\omega_t} + 1\right)} \tag{10}$$

Although the non-resetting part as given in (10) is not a proper function, the completed non-resetting part of Reset PID also consists of integrator and LPFs and hence will be proper. In the case that this is not true, an LPF can be added at a frequency where it does not affect phase at bandwidth, purely to make the function proper.

The frequency response obtained through describing function analysis is compared with that of a linear tamed differentiator in Fig. 5a. It can be seen that for a similar gain behavior, phase at frequencies higher than ω_t is not zero in the case of reset. If $\gamma = 0$ is used, the positive phase achieved would be 52 degrees (as shown in section II).

Since in this case phase addition by reset is after $\omega_t > \omega_c$, it is not useful in adding phase around bandwidth. However, ω_t can be brought closer to ω_d and can even be made equal to ω_d to obtain a $0\,\mathrm{dB}$ gain line with a positive phase, as shown in Fig. 5. Thus, phase addition at bandwidth is done purely through reset and not differentiating action. To compensate for changes in cutoff frequency due to reset (as shown in Fig. 2b), a factor α is used. The reset element can be reformulated as given in (11). γ is chosen such that same phase margin is achieved.

$$\Sigma_r = \frac{1}{\left(\frac{s}{\alpha\omega_d} + 1\right)} \tag{11}$$

It can be observed that the gain at high frequency is lower than the PID, while the low frequency gain is increased, without affecting the phase margin. It can be concluded that theoretically, better tracking and better precision has been achieved while maintaining the same robustness, which was impossible to do with linear control.

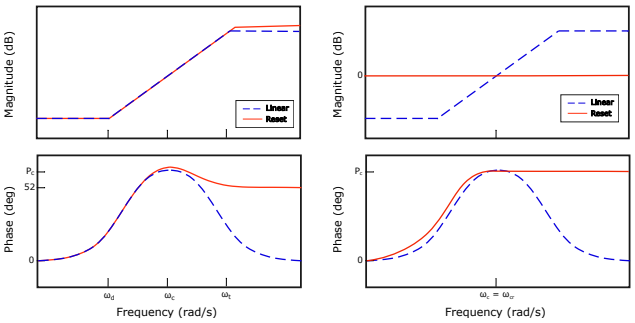

(a) (b)

Fig. 5: (a)Describing function analysis shows positive phase added by reset at frequencies above ω_t when compared to a linear lead component. (b) Reset can be used to achieve the same phase lead with favourable gain behavior.

The reset element, when combined with an integrator and low pass filter, forms Reset PID controller A, given by (12).

$$\Sigma_{RC} = \underbrace{\left(\frac{\alpha\omega_d}{s + \alpha\omega_d}\right)}_{\Sigma_r} \underbrace{K_p \left(1 + \frac{\omega_I}{s}\right)\left(1 + \frac{s}{\omega_d}\right)\left(\frac{\omega_l}{s + \omega_l}\right)}_{\Sigma_{nr}} \tag{12}$$

K_p is chosen such that the open loop gain calculated from describing function analysis equals unity at ω_c .

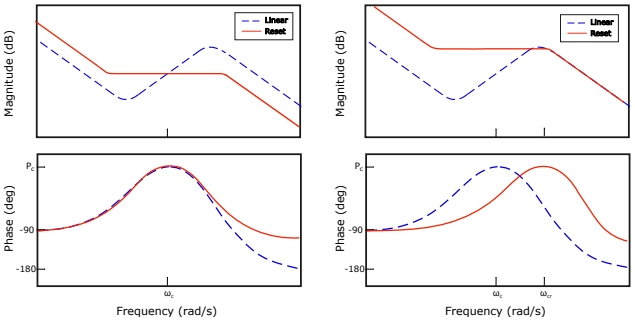

(a) (b)

Fig. 6: (a) Comparison of describing function of Reset PID controller A with a PID controller having the same bandwidth and phase margin. (b) Comparison of describing function of Reset PID controller B with a PID controller having the same precision and phase margin.

By increasing the controller gain such that the gain at high frequencies equals that of PID, an increase in bandwidth can be achieved for the same phase margin and precision as shown in Fig. 6b. It can be seen that bandwidth has increased from ω_c to ω_{cr}. This controller, which provides improved tracking and bandwidth for the same phase margin and precision, will be referred to as Reset PID Controller B. Gain for Controller B at low frequencies is higher than that

of Controller A, thereby indicating a further improvement in tracking performance.

IV. EXPERIMENTAL SETUP

The developed reset PID controller was implemented in the Lorrentz-actuated precision positioning stage shown in Fig. 7a. The coil of the Lorentz actuator is attached to the stator and permanent magnets are mounted on the mover. Parallel leaf flexures are used for the linear guiding of the stage. The position of the stage is measured using a *Renishaw RLE10* laser interferometer with a resolution of $10\,\mathrm{nm}$. Controllers are developed using MATLAB/Simulink environment and are run real time in a dSPACE DS1103 control system, which acts as the interface between the computers and the plant. A sampling rate of $20\,\mathrm{kHz}$ is used for all controllers.

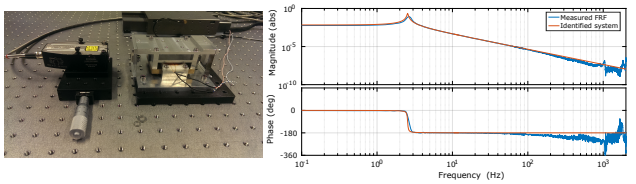

(a) (b)

Fig. 7: (a) Picture of the Lorentz stage (right) with the laser encoder on the left. (b) Frequency response of the system and the identified system model

The frequency response is shown in Fig.7b along with the identified system, which has the behavior of a second order mass-spring-damper system.

V. EXPERIMENTAL VALIDATION

A. Controller Tuning

Controllers A and B are tuned for the precision stage, to have a bandwidth of $150\,\mathrm{Hz}$ and $200\,\mathrm{Hz}$ respectively, with a phase margin of 45°. ω_I is chosen to be $\omega_c/10$, ω_d to be $\omega_c/5$ and $\omega_l = \omega_c * 7$. α is taken as 0.7. K_p is 9.24×10^5 for Controller A and 1.74×10^6 for Controller B.

B. Time Domain Experiments

1) Reference tracking: Fourth-order trajectory planning as formulated in [15] is used to create a triangular wave reference signal with an amplitude of $400\,\mathrm{nm}$. Also, the second-order feedforward proposed in [15] is implemented. Maximum allowed velocity, acceleration, jerk and snap of this reference signal are limited. The tracking errors obtained from the reset controllers are compared with the error from PID in Fig. 8. RMS values of tracking errors are tabulated in Table I. The RMS error for Controller A has reduced by $34\,\%$ compared to PID. This can be explained by the higher low frequency gain of Controller A. The reduction for Controller B is even higher, at around $60\,\%$. This also is as expected, since by increasing bandwidth, the gain of Controller B at lower frequencies is greater than that of controller A.

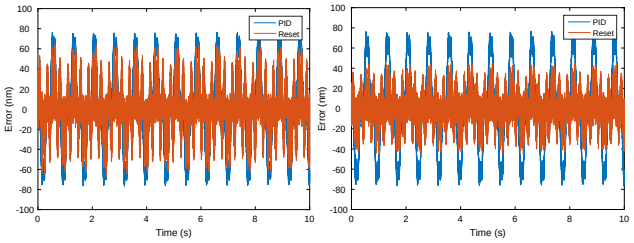

(a) (b)

Fig. 8: (a) Case 1 -Tracking error for Reset controller A vs PID. (b) Case 2 - Tracking error for Reset controller B vs PID.

Controller	Max. Steady State Error (nm)	RMS Tracking Error (nm)
PID	40	41.48
Controller A	20	23.12
Controller B	40	15.73

TABLE I: Comparison of maximum steady state errors and RMS tracking errors for the developed controllers.

2) Steady State Precision: In steady state, with only sensor noise present in the system, the achieved precision was $10\,\mathrm{nm}$ for all the three controllers, which is equal to the resolution of the interferometer used. Therefore, to study the improvement in precision, white noise of amplitude $50\,\mathrm{nm}$ was added as measurement noise n and the error signal was measured. The obtained steady state errors are compared with that of the PID in Fig. 9, and the maximum errors are tabulated in Table I. As expected, Controller A showed reduction in steady state error while Controller B was tuned to have the same precision and hence there was no improvement.

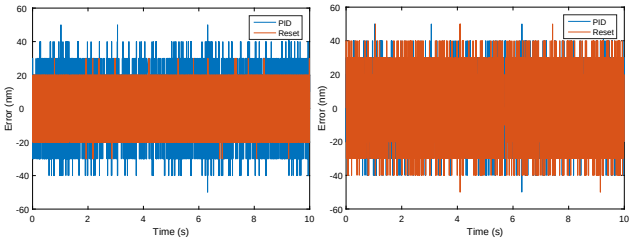

(a) (b)

Fig. 9: (a) Case 1 - Steady error for Reset controller A vs PID. (b) Case 2 - Steady error for Reset controller B vs PID.

C. Frequency Domain Experiments

In order to validate the controllers in frequency domain, a closed loop identification technique was used to compute the sensitivity function $S(j\omega)$ and the complementary sensitivity function $T(j\omega)$. Both $T(j\omega)$ and $S(j\omega)$ were identified by applying a frequency sweep at the measurement noise position n in Fig. 10. $T(j\omega)$ was identified as the transfer

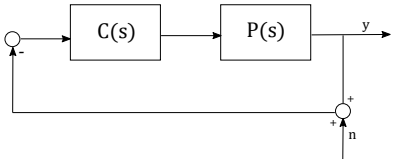

Fig. 10: Block diagram of the control loop with signals $y(t)$ and $n(t)$ used for closed loop identification.

from $-n$ to y, whereas $S(j\omega)$ was identified as the transfer from n to $y+n$.

The identified sensitivity functions for controllers A and B are compared with sensitivity functions estimated from describing function analysis in Fig. 11. Similarly, the complementary sensitivity functions are compared in Fig. 12. It can be seen that the measured responses match well with the estimated responses. From Fig. 12b, it can be seen that the bandwidth has been increased from 150 Hz to around 200 Hz by Controller B, which is an improvement of 33 %. The sensitivity peaks in the identified responses are slightly higher than with describing functions, which shows that reset has added marginally lesser phase than anticipated from describing functions. However, describing function method has been shown to be a good approximation of phase addition by reset in reset PID controllers.

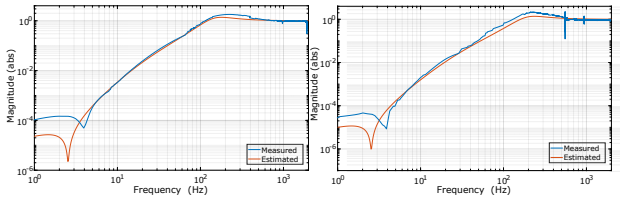

Fig. 11: (a) Comparison of estimated and measured sensitivity function for Controller A (b) Comparison of estimated and measured complementary function for Controller B

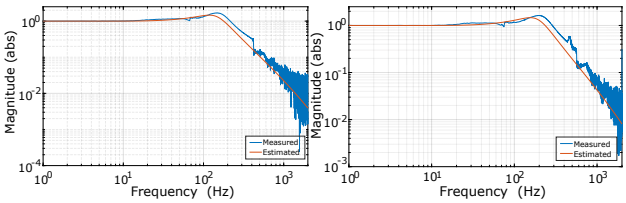

Fig. 12: (a) Comparison of estimated and measured complementary sensitivity function for Controller A (b) Comparison of estimated and measured complementary sensitivity function for Controller B

VI. CONCLUSIONS

In this work a novel reset control method has been proposed in which reset is implemented within the framework of PID, to overcome waterbed effect and achieve better performance. Two reset PID controllers have been developed. The developed controllers were implemented in a high precision positioning setup. Controller A has been shown to provide better tracking and precision than PID, for the same bandwidth. Controller B, as expected from its higher low frequency gain, showed even better tracking and a 33 % improvement in bandwidth for the same precision. The approximations of frequency responses made using describing function analysis are validated by identifying sensitivity function and complementary sensitivity function from the setup. It is shown that the identified responses match well with closed loop responses calculated from describing functions. Thus, the fundamental trade-off between bandwidth and precision in PID has been relaxed, and the severity of water bed effect has been reduced using reset control.

REFERENCES

[1] A. Baos and A. Barreiro, *Reset Control Systems*. Springer Publishing Company, Incorporated, 2013.

[2] S. Skogestad and I. Postlethwaite, *Multivariable Feedback Control: Analysis and Design*. Wiley, 2005. [Online]. Available: https://books.google.nl/books?id=3dxSAAAAMAAJ

[3] R. Schmidt, G. Schitter, and A. Rankers, *The Design of High Performance Mechatronics - 2nd Revised Edition: High-Tech Functionality by Multidisciplinary System Integration*, ser. EBL-Schweitzer. IOS Press, 2014. [Online]. Available: https://books.google.nl/books?id=3WvnAgAAQBAJ

[4] K. Tan, T. Lee, and S. Huang, *Precision Motion Control: Design and Implementation*, ser. Advances in Industrial Control. Springer London, 2007. [Online]. Available: https://books.google.nl/books?id=2UsQob62ihEC

[5] K. strm, "Limitations on control system performance," *European Journal of Control*, vol. 6, no. 1, pp. 2 – 20, 2000. [Online]. Available: http://www.sciencedirect.com/science/article/pii/S094735800070906X

[6] J. C. Clegg, "A nonlinear integrator for servomechanisms," *Transactions of the American Institute of Electrical Engineers, Part II: Applications and Industry*, vol. 77, no. 1, pp. 41–42, March 1958.

[7] Y. Guo, Y. Wang, and L. Xie, "Frequency-domain properties of reset systems with application in hard-disk-drive systems," *IEEE Transactions on Control Systems Technology*, vol. 17, no. 6, pp. 1446–1453, Nov 2009.

[8] H. Li, C. Du, Y. Wang, and Y. Guo, "Discrete-time optimal reset control for the improvement of hdd servo control transient performance," in *Proceedings of the 2009 Conference on American Control Conference*, ser. ACC'09. Piscataway, NJ, USA: IEEE Press, 2009, pp. 4153–4158. [Online]. Available: http://dl.acm.org/citation.cfm?id=1702715.1703015

[9] H. Hosseinnia, I. Tejado, and B. Vinagre, "Fractional-order reset control: Application to a servomotor," vol. 23, p. 781788, 10 2013.

[10] H. Hosseinnia, "A general form for reset control including fractional order dynamics," pp. 2028–2033, 08 2014.

[11] J. Zheng, Y. Guo, M. Fu, Y. Wang, and L. Xie, "Improved reset control design for a pzt positioning stage," in *2007 IEEE International Conference on Control Applications*, Oct 2007, pp. 1272–1277.

[12] N. Saikumar and H. Hosseinnia, "Generalized fractional order reset element (gfrore)," 06 2017.

[13] Y. Li and Y. Wang, "Nonlinear mid-frequency disturbance compensation in hard disk drives," 2005.

[14] L. Hazeleger, M. Heertjes, and H. Nijmeijer, "Second-order reset elements for stage control design," in *2016 American Control Conference (ACC)*, July 2016, pp. 2643–2648.

[15] P. Lambrechts, M. Boerlage, and M. Steinbuch, "Trajectory planning and feedforward design for electromechanical motion systems," vol. 13, pp. 145–157, 02 2005.

[16] A. Gelb and W. E. Vander Velde, *Multiple-input describing functions and nonlinear system design*. New York : McGraw-Hill, 1968, includes bibliographies.